# INFLUENCE OF CONVECTION ON MICROSTRUCTURE 77P

## NAG8 - 753

### Third Semi-annual Progress Report

### 15 August 1989 to 14 February 1990

# CLARKSON UNIVERSITY

## Potsdam, New York 13676

Principal Investigator:    Dr. William R. Wilcox
School of Engineering and
Center for Advanced Materials Processing
(315) 268-6446 or 2336
fax 6438 or 3841


Post-doctoral Research Associate:

Dr. Rubens Caram


Graduate Student Research Assistants:

Mr. A.P. Mohanty, M.S. Candidate in Chemical Engineering
Ms. Jayshree Seth, M.S. Candidate in Chemical Engineering

# SUMMARY

## Goals and objectives

The long range goal of this research is to determine the mechanism responsible for the difference in microstructure caused by solidifying the MnBi-Bi eutectic in space. The objectives for the three year period of the present grant are as follows:

1. Complete the following theoretical analyses:

   a. Determine the influence of the Soret effect on the average solid composition versus distance of off-eutectic mixtures directionally solidified in the absence of convection.

   b. Determine the influence of convection on the microstructure of off-eutectic mixtures using a linear velocity profile in the adjacent melt.

   c. Determine the influence of volumetric changes during solidification on micro-convection near the freezing interface and on microstructure.

   d. Determine the influence of convection on microstructure when the MnBi fibers project out in front of the bismuth matrix.

2. Search for patterns in the effect of microgravity on different eutectics; for example, eutectic composition, eutectic temperature, usual microstructure, densities of pure constituents, and density changes upon solidification.

3. Determine the Soret coefficient and the diffusion coefficient for Mn-Bi melts near the eutectic composition, both through laboratory experiments to be performed here and from data from Dr. David Larson's Shuttle experiments.

## Progress and Plans

The mathematical modeling of fibrous eutectic growth with convection was finished. A paper entitled "Influence of Convection on Rod Spacing of Eutectics" was written and submitted to the Journal of Crystal Growth. The reviewer recommended modest changes which were made and the revised manuscript was submitted.

Progress is being made on determining the influence of the Soret effect on eutectic microstructure without convection. A computer program is now able to calculate the one-dimensional concentration profile resulting from steady-state eutectic solidification in the absence of convection with a realistic temperature profile in the melt. The result of this computation will be used as a boundary condition for calculation of the lateral variation of composition near the solid-liquid interface. (It is this variation of composition that is used to predict the eutectic microstructure in a Hunt-Jackson type treatment.)

A computer program was developed for calculating the concentration profile resulting from holding a liquid in a temperature gradient with Soret thermal diffusion and normal molecular diffusion. This program will be used to interpret the results of our experiments on Mn-Bi melts.

Concentration profiles were obtained for Mn-Bi molten eutectic held in a temperature gradient for different time periods. After long time periods the concentration profiles correspond to those expected theoretically at steady state. From this we can calculate the ratio of the Soret coefficient to the diffusion coefficient. However at short times strange concentration profiles were obtained. We speculate that in heating the eutectic the Bi melted more rapidly so that solid MnBi particles remained for a short time and settled to the bottom of the experimental tube.

A model is being developed for fibrous eutectic solidification with the fibers projecting out into the melt. The differential equations and boundary conditions were established.

In the next six months we expect to complete the theory for the influence of Soret effect on eutectic microstructure with a planar interface and no convection. Work can then begin on the combined influence with convection. The experimental determination of Soret effect in eutectic Mn-Bi will be completed. If Dr. David Larson supplies us with the concentration profiles from his last flight experiment we will use those to help determine the best values for Soret coefficient and diffusion coefficient. A computer program will be developed to calculate the velocity field about fibers projecting into the melt in the presence of laminar shear convection. Then the results will be used to determine the influence on the concentration field.

## INTRODUCTION

This research was inspired by the observation of Dave Larson and Ron Pirich at Grumman that directional solidification of the MnBi-Bi eutectic in space leads to a microstructure finer than when solidification is carried out on earth. This observation held over a wide range of freezing rates. Similar results were obtained on earth by imposing a strong magnetic field on the melt during solidification. Thus the change in microstructure is probably related to the reduced convection expected in space and in a magnetic field. Similar experiments by other investigators on other eutectic melts have given a wide variety of results.

Experiments at Clarkson and at Grumman revealed that the microstructure of MnBi-Bi eutectic is not influenced by the interfacial temperature gradient; thus an altered temperature gradient cannot be responsible for the difference between solidification on earth and in space. Theoretical work at Clarkson led to the prediction that convection during solidification coarsens an eutectic microstructure by altering the concentration field in front of the freezing interface. The theoretical predictions agreed well with experiments using vigorous convection caused by spin-up / spin-down (accelerated crucible rotation technique). However little effect of buoyancy-driven convection was predicted, so that our theory provided no explanation for the Grumman flight results. The theoretical treatment assumed a planar interface, no Soret effect (thermal diffusion), melt composition precisely at the eutectic, equal volumetric properties in all three phases, and rapid interface kinetics. Violation of one or more of these assumptions, as

occurs for real eutectic solidifications, might make the microstructure much more sensitive to convection. Under the current grant we expect to remove some of these conditions in new theoretical treatments.

When a fluid is held in a temperature gradient in the absence of convection, the components slowly separate. This is called "thermal diffusion" for fluids in general, and "the Soret effect" for liquids. When thermal diffusion takes place during solidification, it leads to a change in liquid composition at the freezing interface. This composition change may cause a dramatic alteration in microstructure. Even slight fluid motion may be enough to erase the composition change caused by the Soret effect. We are working on a theoretical treatment of eutectic solidification with Soret effect in the absence of convection. In order to apply a theoretical treatment to the MnBi-Bi eutectic, we must know the Soret coefficient and the diffusion coefficient in these melts. Thus we are working on measuring these physical constants.

Our prior research indicated that the MnBi fibers project out into the melt ahead of the Bi matrix. This may make the concentration field around the fibers more sensitive to convection. Thus we are developing a theoretical treatment for the influence on convection on eutectic microstructure when the fibers project out into the melt.

# I. INFLUENCE OF CONVECTION ON MICROSTRUCTURE

## RUBENS CARAM

## SUMMARY

During this period, the research involved three main objectives:
a. Analysis of convection during eutectic growth.
b. Analysis of thermal diffusion during eutectic growth.
c. Mathematical modeling of thermal diffusion in liquid metals.

The mathematical modeling of fibrous eutectic growth with convection was finished and a paper titled "Influence of Convection on Rod Spacing of Eutectic" was submitted for publication in the Journal of Crystal Growth. The development of a mathematical model to allow one to describe the effect of thermal diffusion on eutectic solidification is partially done. A numerical model to describe thermal diffusion in liquid metals was finished.

## A. INTRODUCTION

During experiments on directional solidification of MnBi-Bi eutectic in space, the microstructure was finer than when solidification was carried out on earth [1-3]. Apparently, these results are due to the reduced convection expected in space. Experiments carried out at Clarkson and at Grumman showed that this microstructure is unchanged by the thermal gradient at the solid/liquid interface. Theoretical work led to the prediction that convection during solidification coarsens an eutectic microstructure by changing the composition of the interfacial liquid [4-8]. However, the changes due to natural convection on earth are expected to be negligible [6].

One of the more reasonable explanations for changes in eutectic microstructure involves thermal diffusion during directional solidification. When a molten alloy is held in a thermal gradient and in the absence of convection, the constituents slowly separate. This is designated thermal diffusion or the Soret effect [9-13]. In eutectic growth, as the solid phases grow they reject atoms into the liquid. This results in a variation of melt composition along the solid/liquid interface and consequently, defines the eutectic microstructure [14-18].

When thermal diffusion occurs during eutectic solidification, it is expected to induces a variation in liquid composition near the freezing interface [17]. This change may cause significant modification in microstructure. Even a small amount of fluid convection may be sufficient to eliminate the composition change produced by the Soret effect. In order to compare theory and experiment for MnBi-Bi eutectic solidification, it is essential to determine the diffusion coefficient and the Soret coefficient in these melts.

The objectives of this work are to:

a. Develop a mathematical model of the influence of convection on the microstructure of a rod-like eutectic.

b. Develop a mathematical model of the influence of the Soret effect during eutectic solidification.

c. Develop a mathematical model for the thermal diffusion in liquid metals.

## B. PROGRESS

### B.1. INFLUENCE OF CONVECTION ON ROD SPACING OF EUTECTIC

The numerical modeling of influence of convection on rod spacing of eutectic was finished. This analysis showed that the spacings between the rods increases with an increase in convection. For the same intensity of convection, an increase in the eutectic composition increases the rod spacing, but the change due to convection is smaller for higher eutectic compositions. Also, it was concluded that the direction of the convective flow plays an important role in changing the rod spacing, since a flow in the y direction provokes a bigger increase in the rod spacing than a flow in the x direction. The results obtained allowed we estimate the effect of natural convection on the microstructure. The value of $\Gamma_0$ computed for a typical experimental set-up is $6.5 \times 10^{-3}$ [8]. For this value, no significant changes were observed. Thus natural convection is not expected to change the spacing between the rods by perturbing the concentration field ahead of the growing interface. The complete results of this work are shown in the appendix I.

### B.2. THE SORET EFFECT IN EUTECTIC SOLIDIFICATION

The purpose of this work is to develop of a mathematical model to describe the influence of the Soret effect during the growth of eutectic alloys. A differential equation describing the compositional field near the interface during unidirectional solidification of a binary eutectic alloy was formulated by including the contribution due to compositional and thermal gradients in the liquid.

Consider the unidirectional solidification of a molten eutectic binary alloy at steady-state, with a phase diagram as shown in figure 1 [10,11]. As the solid/liquid transformation proceeds, two solid phases are grown and the average composition of the frozen solid is the same of the liquid far from the interface, here taken to be the eutectic composition $C_E$. We desire to find the influence of the Soret effect on the solute concentration field in the liquid in front of the solid/liquid interface.

The analysis begins by an interfacial mass balance, as presented in figure 2. The liquid composition $C_L(z)$ is influenced by three factors:

a. Flux due to the compositional gradient:

$$J_1 = -D\frac{\partial C_L}{\partial z} \tag{1}$$

b. Flux due to the advancing solid/liquid interface:

$$J_2 = -VC_L \tag{2}$$

c. Flux due to the temperature gradient:

$$J_3 = -SC_L \frac{\partial T}{\partial z}$$

(3)

where $S$ is the thermal diffusion coefficient, $D$ is the usual molecular diffusion coefficient, $V$ is the rate of displacement of the interface, $dT/dx$ is the thermal gradient in the liquid at the interface and $dC_L/dz$ is the gradient of concentration of solute in the liquid at the interface.

The total flux in the $z$ direction is:

$$J_T = J_1 + J_2 + J_3 = -D \frac{\partial C_L}{\partial z} - VC_L + SC_L \frac{\partial T}{\partial z}$$

(4)

A mass balance over differential element in the liquid yields:

$$\frac{\partial J_T}{\partial z} = -D \frac{\partial^2 C_L}{\partial z^2} - \frac{\partial D}{\partial z} \frac{\partial C_L}{\partial z} - V \frac{\partial C_L}{\partial z} + C_L \frac{\partial S}{\partial z} \frac{\partial T}{\partial z} + SC_L \frac{\partial^2 T}{\partial z^2} + S \frac{\partial C_L}{\partial z} \frac{\partial T}{\partial z}$$

(5)

If $S$ and $D$ are constant with respect to temperature and concentration, equation 5 can be rewritten as:

$$\frac{\partial C_L}{\partial t} = \frac{\partial C_L}{\partial z} = -D \frac{\partial^2 C_L}{\partial z^2} + V \frac{\partial C_L}{\partial z} - S(C_L \frac{\partial^2 T}{\partial z^2} + \frac{\partial T}{\partial z} \frac{\partial C_L}{\partial z})$$

(6)

At the steady-state, $dC_L/dt = 0$, so:

$$D \frac{\partial^2 C_L}{\partial z^2} + V \frac{\partial C_L}{\partial z} - S(C_L \frac{\partial^2 T}{\partial z^2} + \frac{\partial T}{\partial z} \frac{\partial C_L}{\partial z}) = 0$$

(7)

or in three dimensions:

$$D \nabla^2 C_L + V \frac{\partial C_L}{\partial z} - S(C_L \frac{\partial^2 T}{\partial z^2} + \frac{\partial T}{\partial z} \frac{\partial C_L}{\partial z}) = 0$$

(8)

To evaluate the thermal gradient in the melt, it is necessary to determine the temperature profile in the melt. This can be done by solving the heat flow equation which considers a moving interface; it is similar to the mass diffusion equation. For a thin rod, assuming the temperature is function of $z$ only, a heat balance over a differential element gives:

$$KR\frac{\partial^2 T}{\partial z^2} + \rho C_p VR\frac{\partial T}{\partial z} + 2h(T_h - T) = 0 \tag{9}$$

where $K$ is the thermal conductivity, $R$ is the radius of the sample, $\rho$ is the density, $C$ is the thermal capacity, $h$ is the heat transfer coefficient between the rod and the heater, and $T_h$ is the temperature of the heater. We non-dimensionalize by letting:

$$\eta = \frac{z}{R} \tag{10}$$

$$Pe = \frac{\rho C_p VR}{K} \tag{11}$$

$$B = \frac{hR}{K} \tag{12}$$

and

$$\phi = \frac{T - T_h}{T_O - T_h} \tag{13}$$

Then, equation 9 can be written as:

$$\frac{\partial^2 \phi}{\partial \eta^2} + Pe\frac{\partial \phi}{\partial \eta} - 2B\phi = 0 \tag{14}$$

In doing this, we have assumed $T_h$ is constant. For a long rod, the boundary conditions are:
at $\eta = 0$:

$$\phi = 1 \tag{15}$$

and at $\eta \to \infty$:

$$\phi = 0 \tag{16}$$

The solution of equation 13 is:

$$\phi = \exp[-(\frac{Pe + \sqrt{Pe^2 + 8B}}{2})\eta] \tag{17}$$

or

$$T(z) = T_b + (T_b - T_O)\exp(-\Psi z) \tag{18}$$

where $T_O$ is the temperature of the interface, i.e. $T_E$ and $\Psi$ is given by:

$$\Psi = \frac{Pe + \sqrt{Pe^2 + 8B}}{2R} \tag{19}$$

Then, under this condition the derivatives of $T(z)$ are:

$$\frac{\partial T}{\partial z} = \zeta \exp[-\Psi z] \tag{20}$$

$$\frac{\partial^2 T}{\partial z^2} = -\Psi \zeta \exp[-\Psi z] \tag{21}$$

where $\zeta$ is:

$$\zeta = \Psi(T_b - T_E) \tag{22}$$

Substituting this into equation 8, we obtain:

$$\nabla^2 C_L + \frac{V}{D}\frac{\partial C_L}{\partial z} - \frac{S}{D}\zeta\frac{\partial[C_L \exp(-\Psi z)]}{\partial z} = 0 \tag{23}$$

To solve equation 23, it is necessary to determine the average concentration $C_L$ in the liquid far from the solid/liquid interface. This can be done by solving the same equation considering the mass transfer in one dimension only. Then, equation 23 is written as:

$$\frac{\partial^2 \overline{C_L}}{\partial z^2} + \frac{V}{D}\frac{\partial \overline{C_L}}{\partial z} - \frac{S}{D}\zeta\frac{\partial[\overline{C_L}\exp(-\Psi z)]}{\partial z} = 0 \tag{24}$$

Integrating 24:

$$\int \frac{\partial^2 \overline{C_L}}{\partial z^2} dz + \frac{V}{D}\int \frac{\partial \overline{C_L}}{\partial z} dz - \frac{S}{D}\zeta \int \frac{\partial [\overline{C_L} \exp(-\Psi z)]}{\partial z} dz = A \tag{25}$$

Results:

$$\frac{\partial \overline{C_L}}{\partial z} + \overline{C_L}[\frac{V}{D} - \frac{S\zeta \exp(-\Psi z)}{D}] = A_1 \tag{26}$$

The solution of 26 is:

$$\overline{C_L}(z) = \exp[-\frac{V}{D}z - \frac{S\zeta}{D\Psi}\exp(-\Psi z)][A_1 \int \exp[\frac{V}{D}z + \frac{S\zeta}{D\Psi}\exp(-\Psi z)] dz + A_2] \tag{27}$$

The boundary conditions allow one to find $A_1$ and $A_2$:
at $z \rightarrow \infty$:

$$\overline{C_L}(z \rightarrow \infty) = C_E \tag{28}$$

The constant $A_1$ can be found using the L'Hopital rule:

$$\overline{C_L}(z \rightarrow \infty) = \lim \frac{A_1 \int \exp[\frac{V}{D}z + \frac{S\zeta}{D\Psi}\exp(-\Psi z)] dz + A_2}{\exp[\frac{V}{D}z + \frac{S\zeta}{D\Psi}\exp(-\Psi z)]} \tag{29}$$

$A_1$ was found to be $C_E V/D$.
at $z = 0$:

$$\left(\frac{\partial \overline{C_L}}{\partial z}\right)_0 = \frac{SC_E}{D}\left(\frac{\partial T}{\partial z}\right)_0 \tag{30}$$

Then, $A_2$ is $C_E \exp(S\zeta/D\Psi)$
Substituting $A_1$ and $A_2$ in equation 27, we obtain:

$$\overline{C_L}(z) = \exp[-\frac{V}{D}z - \frac{S\zeta}{D\Psi}\exp(-\Psi z)]$$
$$[C_E \frac{V}{D}\int \exp[\frac{V}{D}z + \frac{S\zeta}{D\Psi}\exp(-\Psi z)] dz + C_E \exp(\frac{S\zeta}{D\Psi})] \tag{31}$$

As shown by figure 3, the boundary conditions necessary to solve equation 23 during the growth of a rod-eutectic, are:

At $z \approx \lambda/2$, one should be sufficiently far from the interface that the lateral perturbation of the concentration field is damped out, so that from equation 31:

$$\overline{C_L}(z-\tfrac{\lambda}{2}) = \exp[-\frac{V}{D}z - \frac{S\zeta}{D\Psi}\exp(-\Psi z)]$$

$$[C_E\frac{V}{D}\int \exp[\frac{V}{D}z + \frac{S\zeta}{D\Psi}\exp(-\Psi z)]dz + C_E\exp(\frac{S\zeta}{D\Psi})] \tag{32}$$

A material balance at $z = 0$ over the $\alpha$ phase yields:

$$\left(\frac{\partial C_L}{\partial z}\right)_0 = -\frac{V}{D}(C_{L_0} - C_s^\alpha) + C_{L_0}\frac{S}{D}\frac{\partial T}{\partial z} \tag{33}$$

or

$$\left(\frac{\partial C_L}{\partial z}\right)_0 = -\frac{V}{D}(C_{L_0} - C_s^\alpha) + C_{L_0}\frac{S}{D}\zeta\exp[-\Psi z] \tag{34}$$

Similarly a material balance at $z = 0$ over the $\beta$ phase gives:

$$\left(\frac{\partial C_i}{\partial z}\right)_0 = -\frac{V}{D}(C_{L_0} - C_s^\beta) + C_{L_0}\frac{S}{D}\frac{\partial T}{\partial z} \tag{35}$$

or

$$\left(\frac{\partial C_i}{\partial z}\right)_0 = -\frac{V}{D}(C_{L_0} - C_s^\beta) + C_{L_0}\frac{S}{D}\zeta[-\Psi z] \tag{36}$$

Since the rod structure repeats itself periodically in both x and y directions, the computational domain will be a rectangular area as presented in figure 4. Under such a case, the other boundary conditions are:

$$C_L^{x=0} = C_L^{x=\lambda} \tag{37}$$

and

$$C_L^{\gamma=0} - C_L^{\gamma=\sqrt{3}\lambda} \qquad (38)$$

The next phase of this work includes the solution of equation 23 for rod-like eutectic solidification. Since an analytical solution is not likely to be obtained, a numerical model based on central finite difference should be employed. To solve the problem, the boundary conditions will be given by equations 32, 34, 36, 37 and 38.

## B.3. THE SORET EFFECT IN MOLTEN BINARY ALLOY

The thermal diffusion or the Soret effect is the relative movement of components in a mixture due to an applied temperature gradient. The main purpose of this work is to develop a mathematical treatment for the compositional changes in a molten binary alloy sample held in a thermal gradient. The results allow one to find the transport coefficients from experimental data.

Consider a sample of a molten binary alloy of homogeneous composition $C_O$. When there is a thermal gradient in this system, it will induce a mass flux known as the Soret effect. Since the Soret effect will change the composition profile along the sample, it indirectly gives rise to an opposing mass flux due to the composition gradient. Then, in absence of convection, the composition of the liquid is influenced by two forms of mass transport:

a. Mass flux due to the composition gradient:

$$J_1 = -D\frac{\partial C_L}{\partial x} \qquad (39)$$

b. Mass flux due to the thermal gradient:

$$J_2 = SC_L\frac{\partial T}{\partial x} \qquad (40)$$

According to figure 5, the total mass flux $J_T$ in the x direction is given by:

$$J_T = J_1 + J_2 = -D\frac{\partial C_L}{\partial x} + SC_L\frac{\partial T}{\partial x} \qquad (41)$$

Thus the rate of change of concentration at a point is given by:

$$\frac{\partial C_L}{\partial t} - \frac{\partial J_T}{\partial x} = -\frac{\partial D}{\partial x}\frac{\partial C_L}{\partial x} - D\frac{\partial^2 C_L}{\partial x^2} + C_L\frac{\partial T}{\partial x}\frac{\partial S}{\partial x} + C_L S\frac{\partial^2 T}{\partial x^2} + S\frac{\partial T}{\partial x}\frac{\partial C_L}{\partial x} \qquad (42)$$

If $D$ and $S$ are constant with respect to temperature and composition, equation 42 can be rewritten as:

$$\frac{\partial C_L}{\partial t} = -D\frac{\partial^2 C_L}{\partial x^2} + C_L S\frac{\partial^2 T}{\partial x^2} + S\frac{\partial T}{\partial x}\frac{\partial C_L}{\partial x} \qquad (43)$$

In order to determine the variation of the liquid composition as a function of time and distance, equation 43 should be solved. The initial composition is $C_O$ and the boundary conditions for this problem are obtained by noting that there can be no net flux through the ends of the sample, or $J_T = 0$ at $x = 0$ and at $x = L$:

$$\left(\frac{\partial C_L}{\partial x}\right)_0 = \frac{S}{D}C_{L_0}\frac{\partial T}{\partial x} \qquad (44)$$

$$\left(\frac{\partial C_L}{\partial x}\right)_L = \frac{S}{D}C_{L_L}\frac{\partial T}{\partial x} \qquad (45)$$

To solve the governing partial differential equation, an explicit finite difference scheme was applied. In order to reduce the numerical computation and to more immediately exhibit the form the results should take, equation 43 was non-dimensionalized. Then, equation 6 becomes:

$$\frac{\partial \omega}{\partial \tau} = -\frac{\partial^2 \omega}{\partial \chi^2} + \omega\Phi\frac{\partial^2 \pi}{\partial \chi^2} + \Phi\frac{\partial \pi}{\partial \chi}\frac{\partial \omega}{\partial \chi} \qquad (46)$$

where $\chi = x/L$, $\omega = C_L/C_O$, $\tau = tD/L^2$, $\Phi = S(T-T_0)/D$ and $\pi = (T - T_0)/(T_L - T_0)$ where $T_0$ and $T_L$ are the temperatures of the ends of the sample. The boundary conditions become: at $\chi = 0$:

$$\left(\frac{\partial \omega}{\partial \chi}\right)_0 = \Phi\omega_0\left(\frac{\partial \pi}{\partial \chi}\right)_0 \qquad (47)$$

at $\chi = 1$:

$$\left(\frac{\partial \omega}{\partial \chi}\right)_1 - \Phi \omega_1 \left(\frac{\partial \pi}{\partial \chi}\right)_1 \tag{48}$$

The one dimensional grid formed for the problem is represented in figure 6. The three point central difference forms were used for the first and second derivatives:

$$\frac{\partial \omega}{\partial \chi} - \frac{\omega_{i+1} - \omega_{i-1}}{2\Delta\chi} \tag{49}$$

$$\frac{\partial^2 \omega}{\partial \chi^2} - \frac{\omega_{i+1} + \omega_{i-1} - 2\omega_i}{\Delta\chi^2} \tag{50}$$

and for the derivative with respect to the time:

$$\frac{\partial \omega}{\partial \tau} - \frac{\omega_i^* - \omega_i}{\Delta\tau} \tag{51}$$

where $\omega^*$ is the liquid composition after a period $\Delta\tau$.

Substituting difference equations 49 to 51 into the differential equation 46:

$$\frac{\omega_i^* - \omega_i}{\Delta\tau} - -\left(\frac{\omega_{i+1} + \omega_{i-1} - 2\omega_i}{\Delta\chi^2}\right) + \omega_i \Phi \frac{\partial^2 \pi}{\partial \chi^2} + \left(\Phi \frac{\partial \pi}{\partial \chi} \frac{\omega_{i+1} - \omega_{i-1}}{2\Delta\chi}\right) \tag{52}$$

or

$$\omega_i^* - M\left(\Phi \Delta\chi \frac{\partial \pi}{\partial \chi} - 2\right)\omega_{i+1} - M\left(\Phi \Delta\chi \frac{\partial \pi}{\partial \chi} + 2\right)\omega_{i-1}$$

$$+ M\left(4 + 2\Phi \Delta\chi^2 \frac{\partial^2 \pi}{\partial \chi^2} + \frac{1}{M}\right)\omega_i \tag{53}$$

where $M$ is given by:

$$M - \frac{\Delta\tau}{2\Delta\chi^2} \tag{54}$$

The boundary conditions become:

at $\chi = 0$:

$$\omega_{i-1} - \omega_{i+1} - 2\Delta\chi \Phi \omega_i \left(\frac{\partial \pi}{\partial \chi}\right)_0 \qquad (55)$$

at $\chi = 1$:

$$\omega_{i+1} - 2\Delta\chi \Phi \omega_i \left(\frac{\partial \pi}{\partial \chi}\right)_1 + \omega_{i-1} \qquad (56)$$

For the case of a constant temperature gradient, at the end of the process, when the thermal gradient flux and compositional gradient flux cancel out, a steady-state is reached ($\partial C/\partial t = 0$). The solution for this case can be found analytically by solving:

$$\frac{\partial^2 \omega}{\partial \chi^2} - \Phi \frac{\partial \pi}{\partial \chi} \frac{\partial \omega}{\partial \chi} = 0 \qquad (57)$$

Considering $C_O$ the initial composition of the sample, the liquid concentration as function of distance is given by:

$$\omega(\chi) = \Phi \frac{\partial \pi}{\partial \chi} \frac{e^{\Phi \frac{\partial \pi}{\partial \chi}\chi}}{\left(e^{\Phi \frac{\partial \pi}{\partial \chi}} - 1\right)} \qquad (58)$$

Figure 7 shows concentration profiles for several value of dimensionless time $\tau$.

## C. PLANS

For the next phase of this project, the mathematical modeling of the thermal diffusion during eutectic solidification should be finished. A numerical model that allows one to simulate the eutectic growth and consequently the investigation of large range of parameters is expected to be done. A steady-state solution of the differential equation will be obtained by applying appropriate boundary conditions and accounting for heat flow in the melt. To solve the problem, a numerical model based on central finite difference technique will be developed. Following that, the average interfacial composition will be converted to a variation of undercooling at the interface, and consequently to microstructural parameters. Also, the mathematical analysis of the Soret effect diffusion in liquid metals is planned to be completed and this will permit the analysis of experimental data and the theoretical provided by the model.

## D. REFERENCES

[1] R. G. Pirich and D.J. Larson, in: Materials Processing in Reduced Gravity Environment

of Space, Ed. G.E. Rindone (North - Holland, New York, 1982) p. 253.

[2] R. G. Pirich, G, Bush, W. Poit and D.J. Larson, Jr, Met. Trans. 11A (1980) 193.

[3] G. Muller and P. Kyr, in: Proc. 15th European Symp. on Materials Science under Microgravity, Schloss Elmau, Nov. 1984, ESA SP-222, p.141.

[4] V. Baskaran and W.R. Wilcox, J. Crystal Growth 67 (1984) 343.

[5] S. Chandrasekhar, PhD Thesis, Clarkson University, Potsdam (1987).

[6] R. Caram, S. Chandrasekhar and W.R.Wilcox, to be published, J. Crystal Growth.

[7] S. Chandrasekhar, G.F. Eisa and W.R. Wilcox, J. Crystal Growth 78 (1986) 485.

[8] G. F. Eisa and W.R. Wilcox, J. Crystal Growth 78 (1986) 159.

[9] A. S. Yue, J. Crystal Growth 42 (1977) 542.

[10] A. S. Yue, J. Phys. Chem. Solids Suppl. 328 (1967) 197.

[11] A. S. Yue and J. T. Yue, J. Crystal Growth 13/14 (1972) 797.

[12] J. C. Legros, P. Goemaere and J. K. Platten, Phys. Rev. 32A (1985) 1903.

[13] D. T. J. Hurle, J. Crystal Growth 61 (1983) 463.

[14] K. A. Jackson and J.D. Hunt, Trans. AIME 2368 (1966) 1129.

[15] M. A. Savas and R. W. Smith, J. Crystal Growth 76 (1986) 880.

[16] R. Trivedi, P. Magnin and W. Kurz, Acta Metall. 35 (1987) 971.

[17] J. D. Verhoeven, J. C. Warner and E. D. Gibson, Met. Trans. 3A (1972) 1437.

[18] R. G. Pirich, Met. Trans. 15A (1984) 2139.
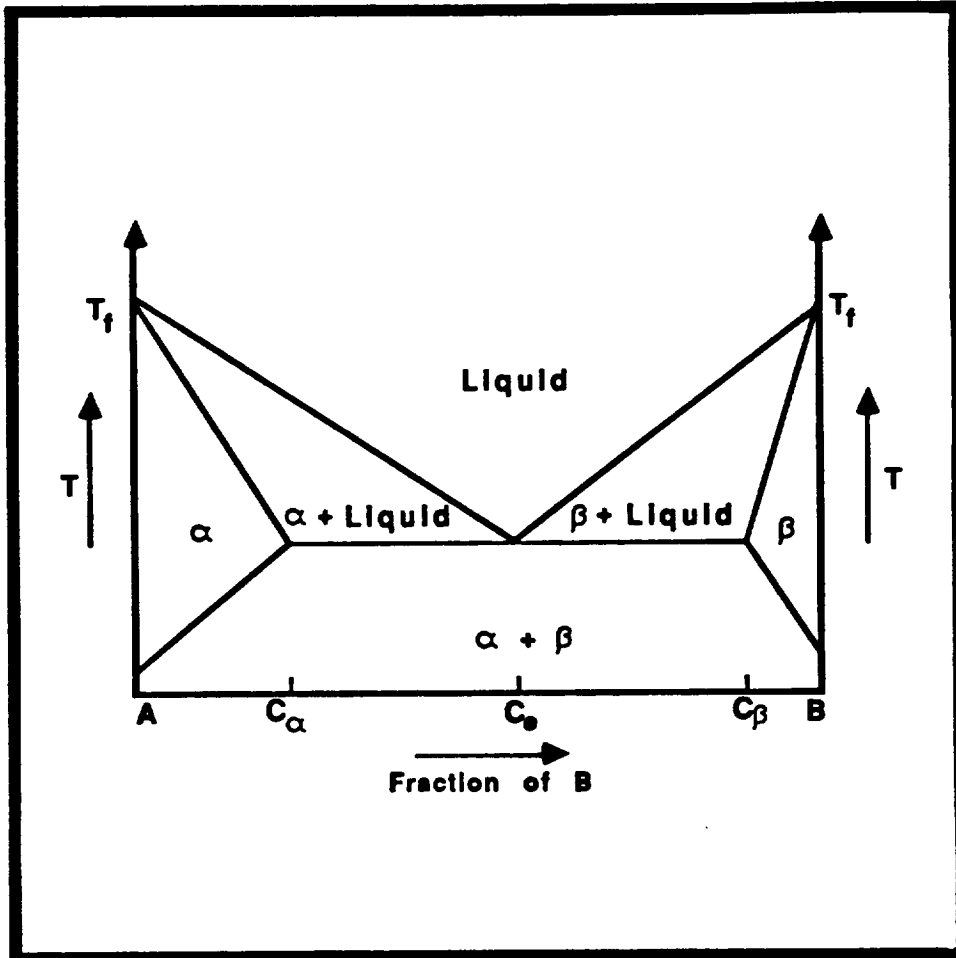
Figure 1. Schematic of typical simple eutectic phase diagram.
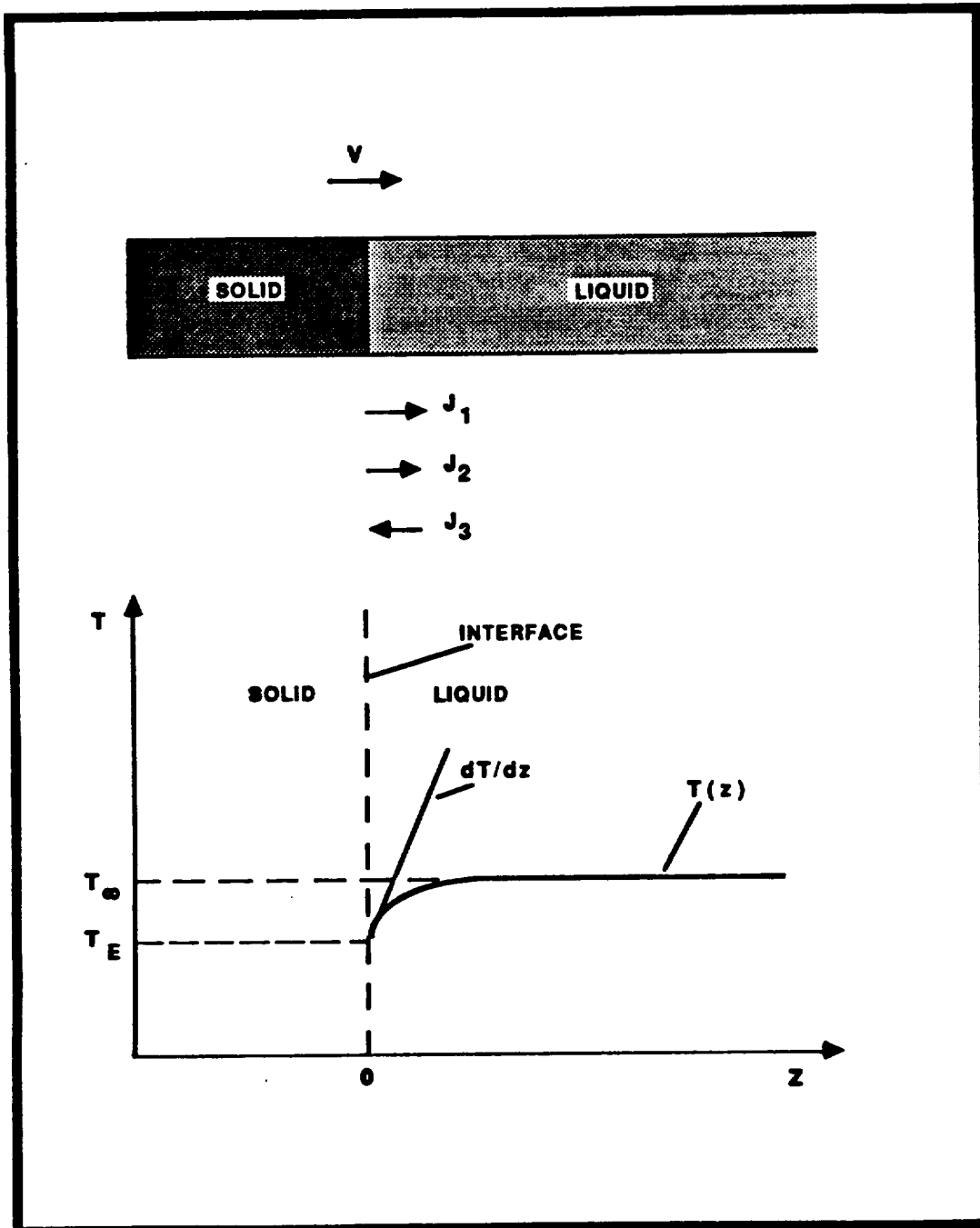
Figure 2. Diagram of temperature profile and fluxes $(J_1, J_2, J_3)$ at the interface.
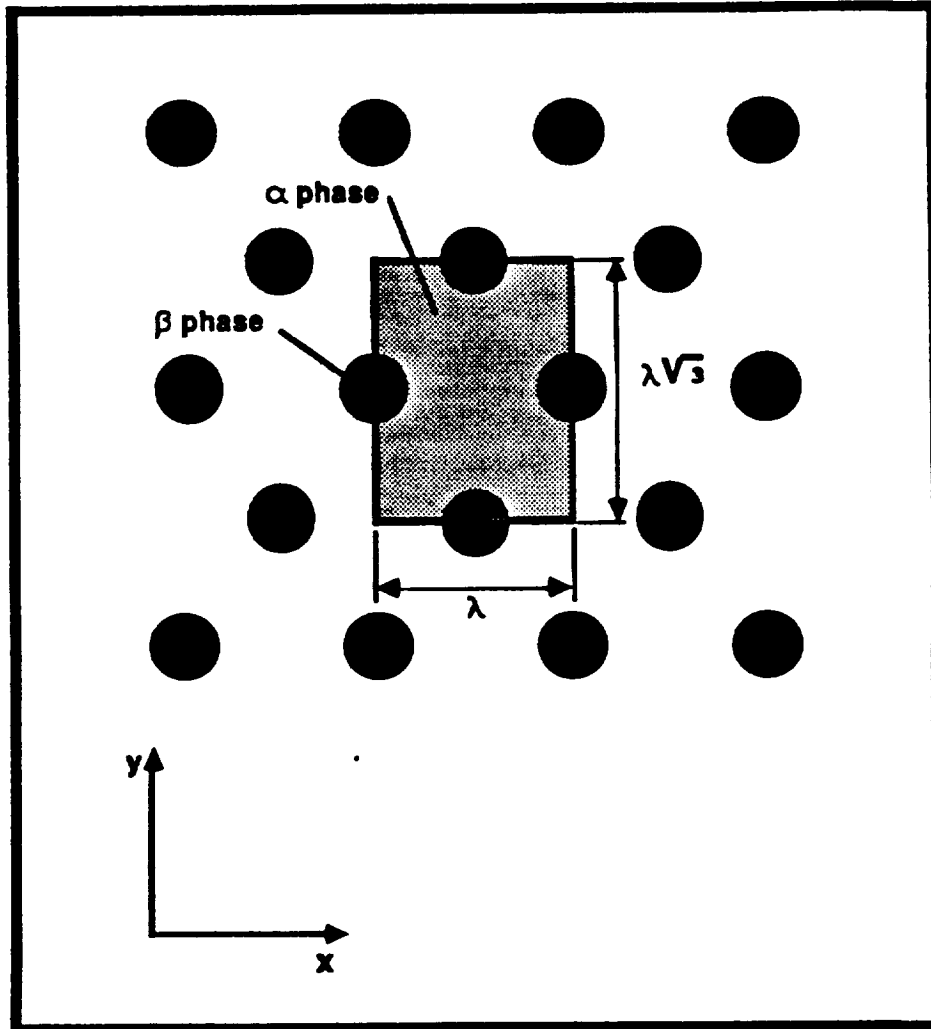
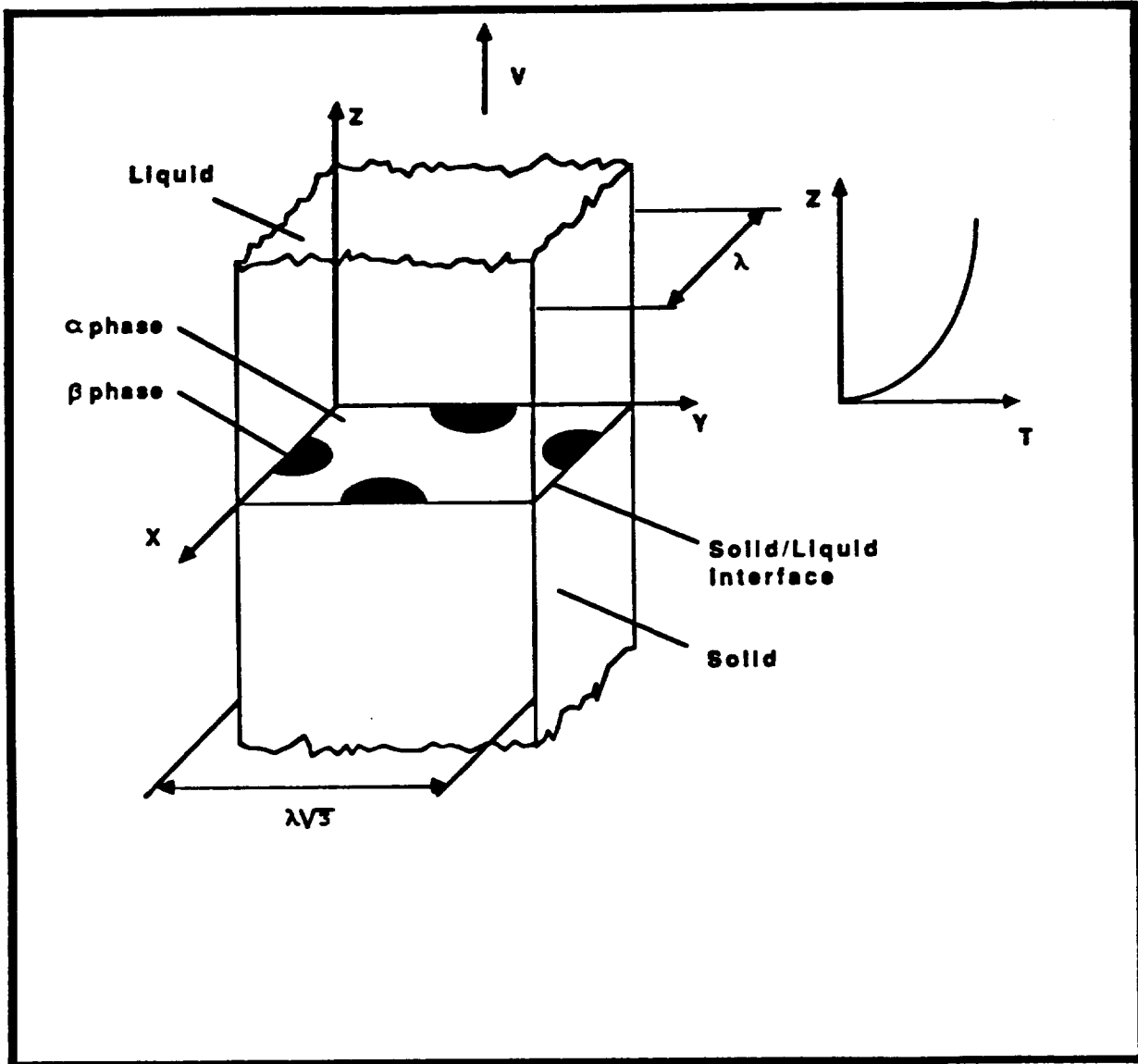Figure 3. A rod eutectic structure viewed normal to the freezing interface.

Figure 4. A three dimensional view of the liquid near the interface of rod eutectic structure viewed normal to the freezing interface.
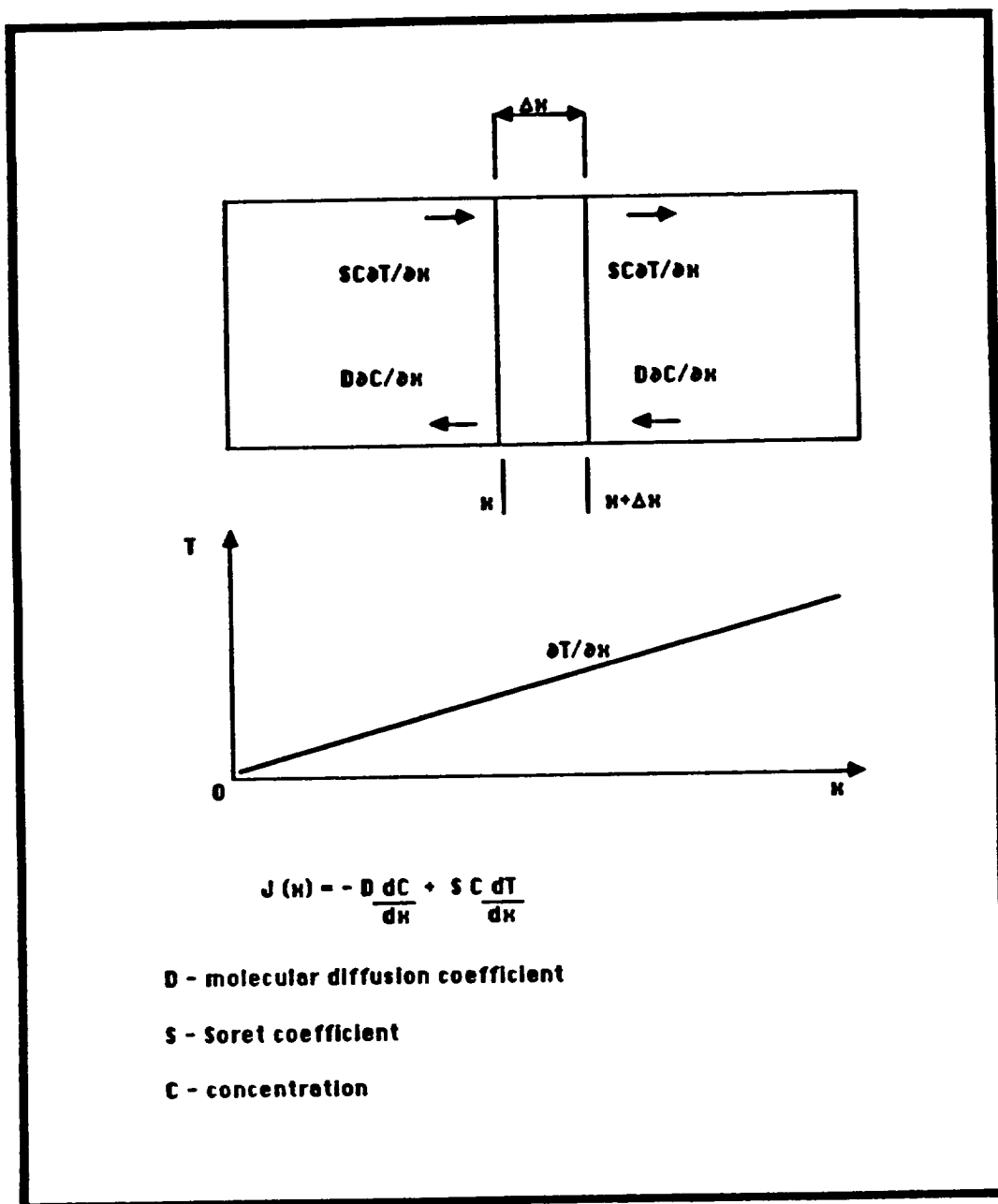
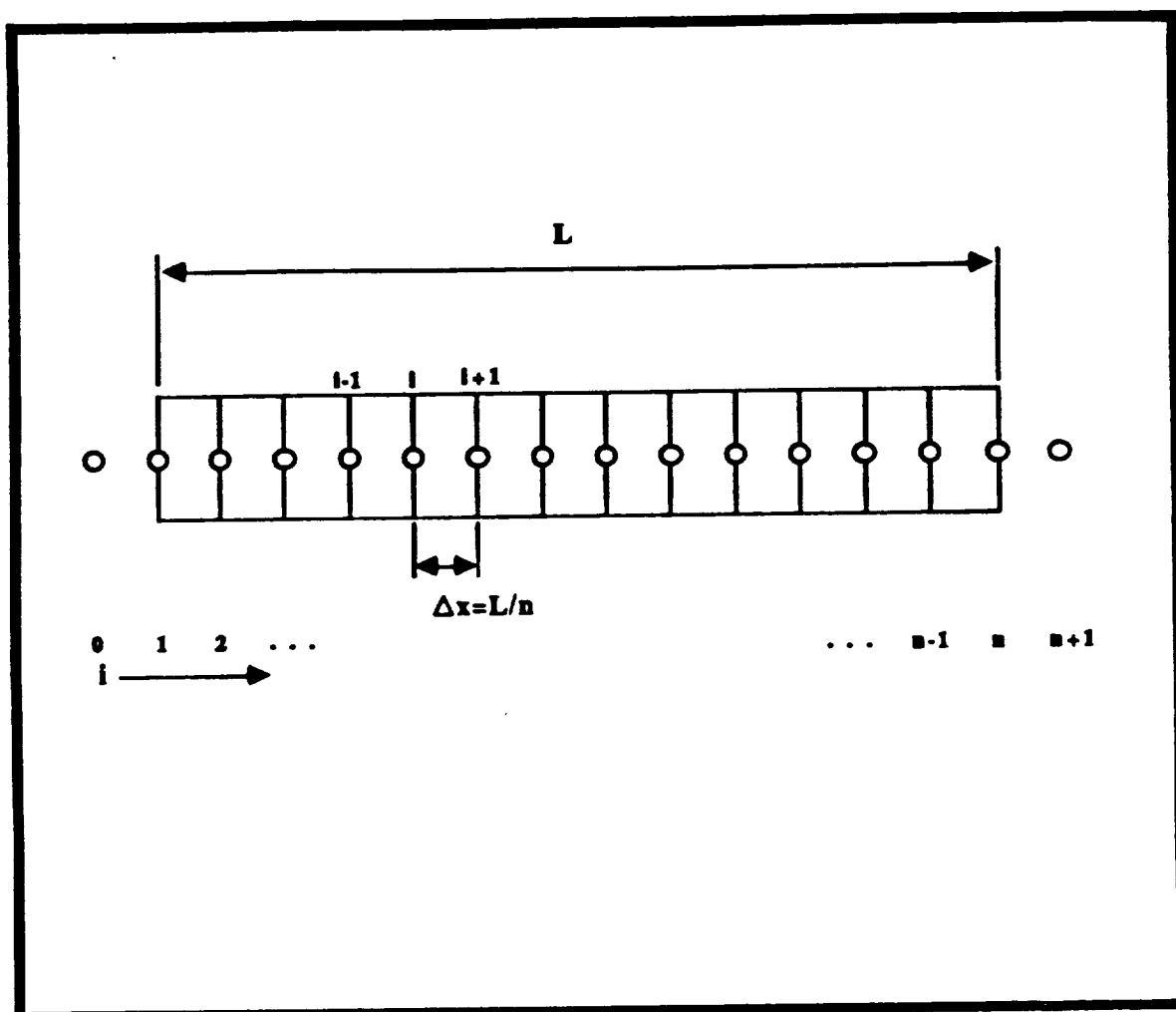Figure 5. Diagram of mass transfer in a molten binary alloy.

Figure 6. Finite difference grid used to model numerically the Soret effect in a molten binary alloy.
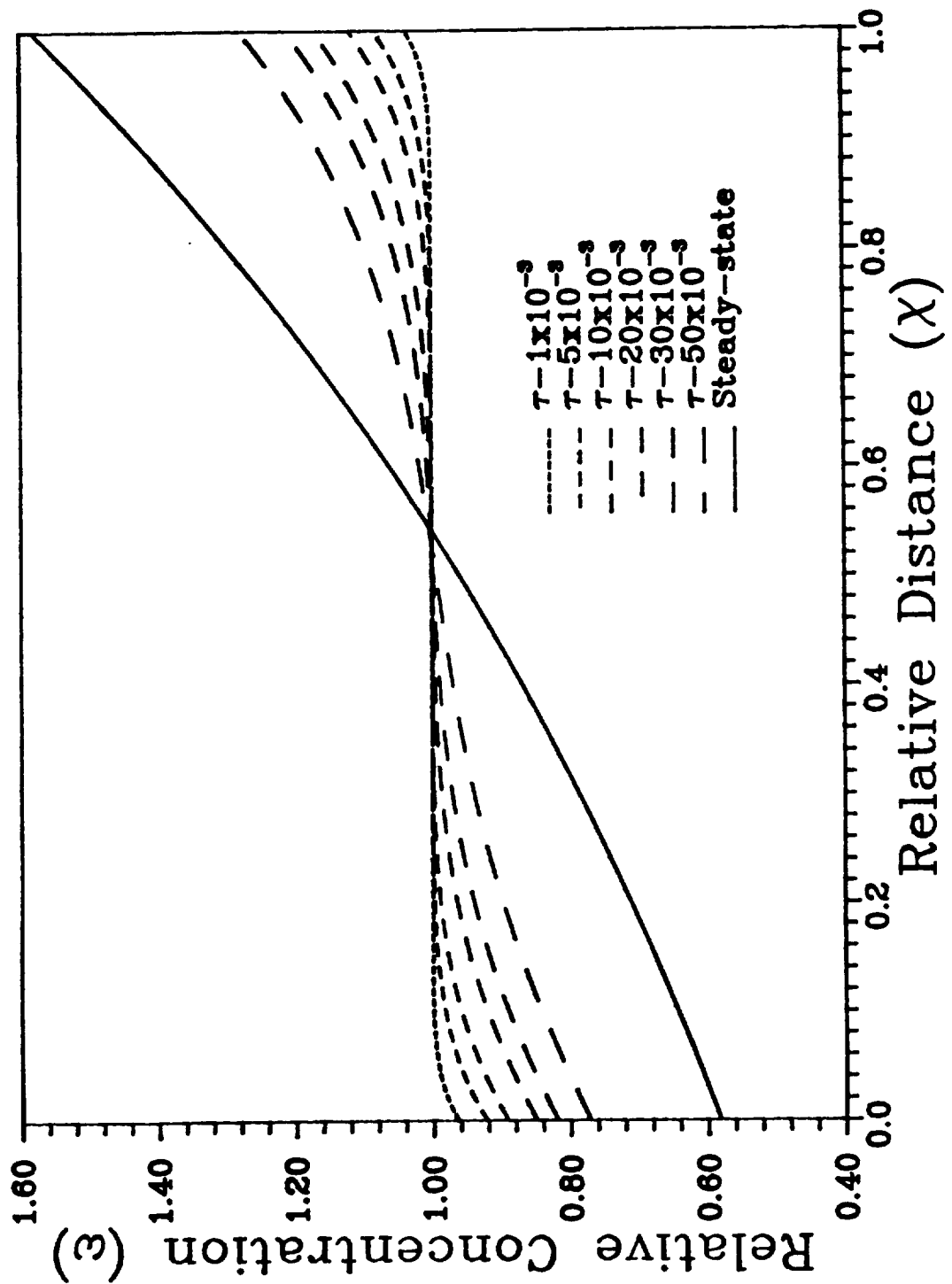
Figure 7.a. Relative concentration in a molten binary alloy as a function of relative distance, for several diffusion periods, $\Phi = 10^{-1}$ and $\partial\pi/\partial\chi = 10$.
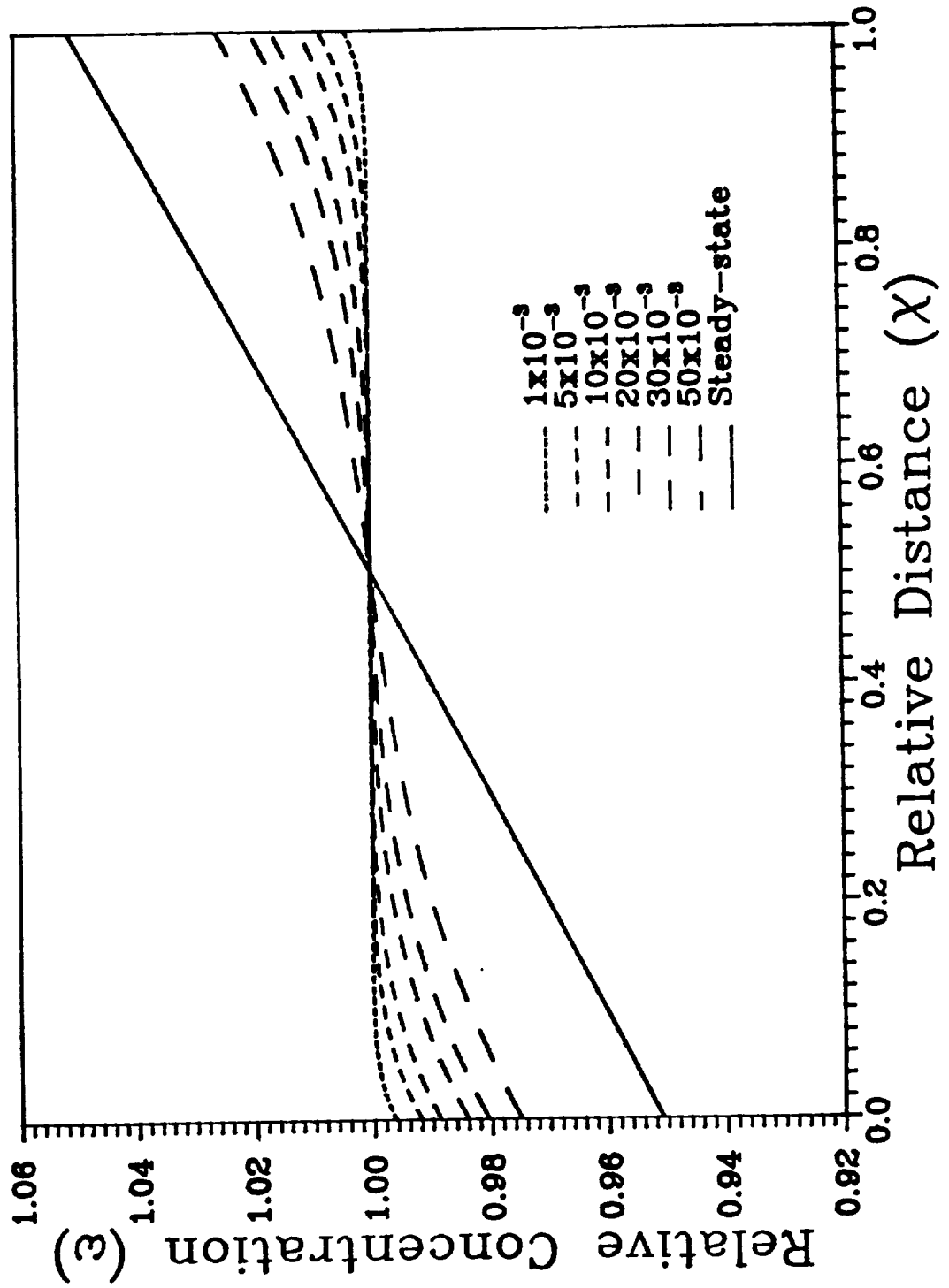
Figure 7.b. Relative concentration in a molten binary alloy as a function of relative distance, for several diffusion periods, $\Phi = 10^{-2}$ and $\partial \pi / \partial \chi = 10$.

Figure 7.c. Relative concentration in a molten binary alloy as a function of relative distance, for several diffusion periods, $\phi = 10^3$ and $\partial \pi / \partial \chi = 10$.
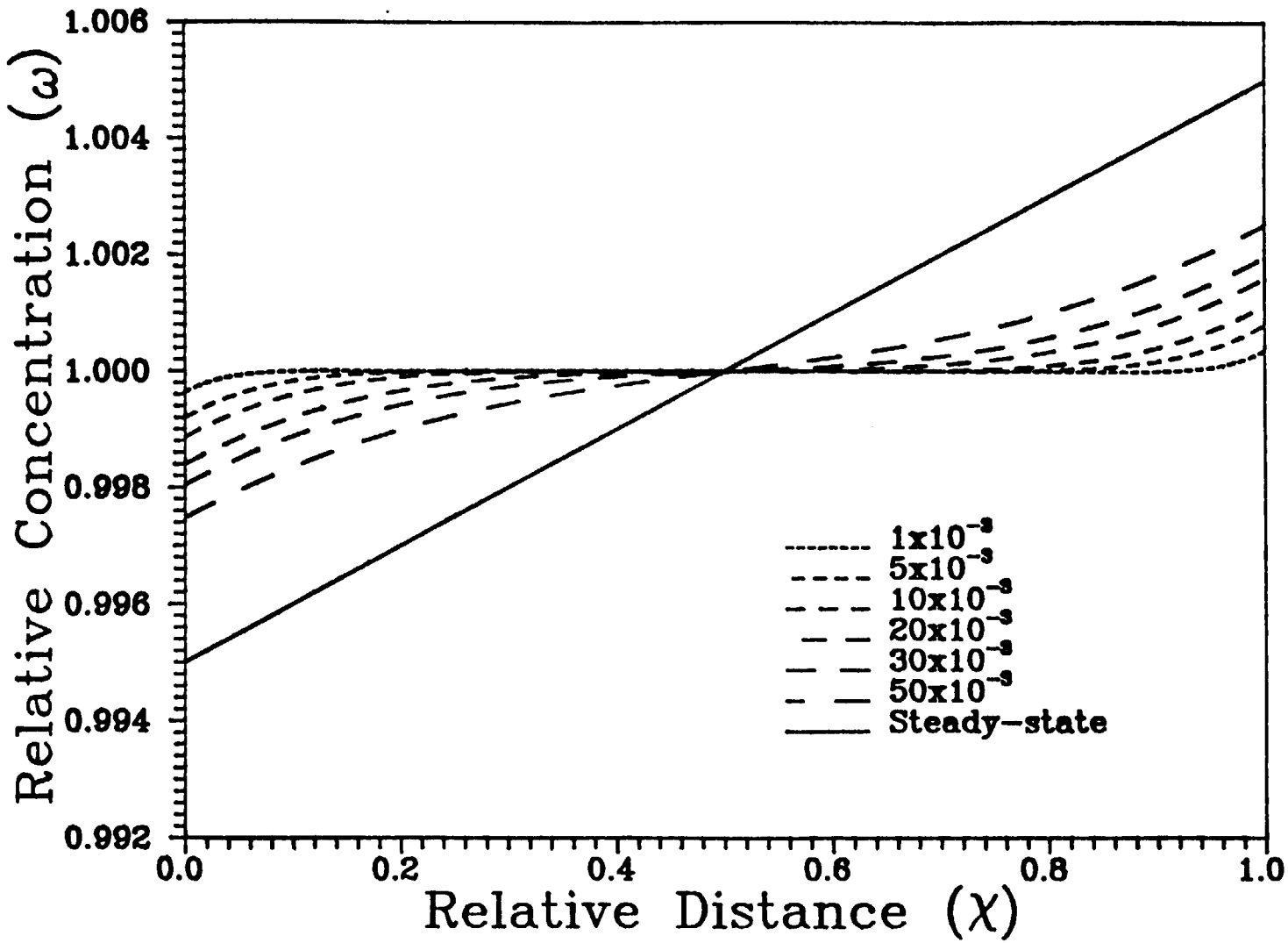
APPENDIX I

(Submitted to the Journal of Crystal Growth)

# INFLUENCE OF CONVECTION ON ROD SPACING OF EUTECTICS

R. Caram[*], S. Chandrasekhar[**] and W.R. Wilcox

Clarkson University, Potsdam, NY 13699, USA

## ABSTRACT

This paper describes a three dimensional numerical model to study the influence of convection on the rod-like microstructure of an eutectic system. This model is based on a central finite difference approach. By applying it, the average concentration near the solid/liquid interface of a growing rod-like eutectic was determined for eutectic compositions $C_e$ of 0.03, 0.05 and 0.10. Following Jackson and Hunt, the average interfacial composition was converted to a change of undercooling at the interface and, finally, to spacing between the rods. The change in rod spacing with increasing intensity of convection was calculated assuming the eutectic grows at minimum interfacial undercooling. It was confirmed that an increase in convection should coarsen the microstructure, i.e. the rod spacing increases with increasing intensity of stirring. The direction of the convection relative to the rod array is a very important parameter in such an analysis.

Present addresses : [*] State University of Campinas, Brazil.

[**] Quantum Technologies, Inc., Sanford, FL 32771

## 1. INTRODUCTION

In recent years, a new class of materials, classified as composites, has been increasing in importance. Composites offer the exceptional advantage of being able to combine the properties of different components into one material. Applying the process of directional solidification of eutectic alloys, it is possible to produce in-situ composites which have high degree of thermal stability and better properties than their individual components.

During the solidification process, mass transfer by convection may play a significant role in determining the eutectic microstructure and thereby the properties. Considering such facts, the development of a simulation model which allows evaluation of the influence of convection on the eutectic microstructure is important. The inspiration to perform this work came from the results obtained from experiments in space, where the solidification of the eutectic alloys MnBi-Bi[1,2] and InSb-NiSb[3] showed a decreased spacing between the rods compared to earth processed samples grown at identical growth rates. Prior theoretical work on the effect of convection on the growth of lamellar eutectics predicted that the spacing between the lamellae increases with increasing convection[4,5]. However, we expected that the rod structure might be more sensitive to convection than the lamellar structure. The main purpose of the present work is to present a three-dimensional mathematical model to describe the influence of convection on the microstructure of rod-like eutectics by calculating the average melt concentration over the $\alpha$ and $\beta$ solid phases.

## 2. MATHEMATICAL MODELLING

In order to develop this analysis, a typical structure of a rod-like eutectic was selected, as shown in figure 1, where a normal view to its interface is presented. The rods are placed on the corners of a hexagon as assumed by Jackson and Hunt[6].

During an eutectic solidification, as the solid phases grow they reject atoms to the melt and the result is variation of liquid composition along the solid/liquid interface. At steady state, mass transfer in the absence of convection is governed by the differential equation:

$$\nabla^2 C + (V/D)\partial C/\partial z = 0 \tag{1}$$

where C is the composition of the melt, V is the rate of displacement of the solid/liquid interface and D is the diffusion coefficient of the solute. An analytical solution of equation 1 was obtained by Jackson and Hunt[6], who used the concentration field to calculate the average undercooling at the interface and the rod spacing.

To account for the influence of convection, a transverse flow U is assumed across the interface in the x and y directions, as presented in figure 2. Using the symbols defined at the end of the paper, the differential equation for continuity of mass at steady-state becomes :

$$\nabla^2 C + (V/D)\partial C/\partial z - (G_{Ux}z/D)\partial C/\partial x - (G_{Uy}z/D)\partial C/\partial y = 0 \tag{2}$$

in which the lateral flow is assumed to have a constant velocity gradient $G_U = dU/dz$ over the smallest region which satisfies a periodicity condition for the rods.

To solve equation 2, a numerical model based on a central finite difference approach was developed. In order to make this mathematical treatment, the interface of the domain of interest was divided into two

phases ($\alpha$ and $\beta$) according to the lever rule. Each rod's cross-section ($\beta$ phase) was approximated by an array of rectangular elements, since this facilitated the use of Cartesian coordinates to model the problem. As in all prior theoretical work, it was implicitly assumed that the volumetric properties are the same in all three phases. Also, the interface was assumed to be planar.

The boundary conditions are :

at z = $\lambda$/2, where $\lambda$ is the spacing between the rods,

$$C = C_e \tag{3}$$

at z = 0, and over the $\alpha$ phase,

$$D(\partial C/\partial z) = -V(C_i - C_\alpha) \tag{4}$$

at z = 0, and over the $\beta$ phase,

$$D(\partial C/\partial z) = -V(C_i - C_\beta) \tag{5}$$

Several values of z were tried for the far field boundary condition. With z = $\lambda$, the melt composition over the solid phases changed only in the 5th decimal place for z > $\lambda$/2, and so it was decided to use z = $\lambda$/2 for the far field boundary condition. The computational domain represents a small section of the periodic array of rods. Thus it was assumed that the composition field repeats itself in both the x and y directions :

$$C_{x=0} = C_{x=\lambda} \tag{6}$$

and

$$C_{y=0} = C_{y=\sqrt{3}\lambda} \tag{7}$$

Solid solubility was assumed to be negligible and hence $C_\alpha$ = 0 and $C_\beta$ = 1. The differential equation was non-dimensionalized to reduce the number of variables to two for a fixed eutectic composition. The scaling

variables are similar to those used by Baskaran and Wilcox[4], i.e. $X=x/\lambda$, $Y=y/\lambda$ and $Z=z/\lambda$. The non-dimensional equation is :

$$\nabla^2 C + A\partial C/\partial Z - \Gamma_x Z\partial C/\partial X - \Gamma_y Z\partial C/\partial Y = 0 \qquad (8)$$

Where $\Gamma$ is a rod spacing based Peclet number and $A$ is the dimensionless convective velocity gradient at the interface. For typical experimental rod eutectic growth with forced convection, $A \approx 0.05$ and $\Gamma \approx 280$[7]. The boundary conditions become :

at $Z = 1/2$,

$$C = C_e \qquad (9)$$

at $Z = 0$ over the $\alpha$ phase,

$$dC/dZ = -A(C_i - C_\alpha) \qquad (10)$$

at $Z = 0$ over the $\beta$ phase,

$$dC/dZ = -A(C_i - C_\beta) \qquad (11)$$

The periodicity conditions in the x and y directions are:

$$C_{X=0} = C_{X=1} \qquad (12)$$

and

$$C_{Y=0} = C_{Y=\sqrt{3}} \qquad (13)$$

The principal result of this analysis required to evaluate the change of fiber spacing due to convection is the average concentration of the interfacial liquid over each solid phase. This was done numerically by calculating the average concentration over the area formed by the grid points of the two phases.

## 3. RESULTS and DISCUSSION

Figure 3.a is a three-dimensional plot of the computed concentration in the domain for an eutectic composition of $C_e = 0.05$ growing without the disturbing influence of convection. Convection

distorts the contours, as shown in figure 3.b and 3.c for $\Lambda = 0.05$ and $\Gamma = 280$.

The relationship between convection and the spacing between the rods is obtained by modifying the Jackson and Hunt analysis to include a perturbation in the concentration field due to convection, $\Delta$. Thus the perturbation in the concentration field in the $\alpha$ and $\beta$ phases are :

$$\Delta_\alpha = (C_{i\alpha}^* - C_e)_0 - (C_{i\alpha}^* - C_e) \tag{14}$$

and

$$\Delta_\beta = (C_e - C_{i\beta}^*)_0 - (C_e - C_{i\beta}^*) \tag{15}$$

where the index 0 means no convection and $C_{i\alpha}^*$ and $C_{i\beta}^*$ are the average interfacial melt compositions over the $\alpha$ phase and the $\beta$ phase respectively.

In the absence of convection, the deviation of the average interfacial composition from the eutectic is proportional to $\Lambda = \lambda V/D$, so,

$$(C_{i\alpha}^* - C_e) = A_\alpha \Lambda \tag{16}$$

and

$$(C_e - C_{i\beta}^*) = A_\beta \Lambda \tag{17}$$

For circular rods in a circular array the values of $A_\alpha$ and $A_\beta$ can be obtained from the analytical solution of Jackson and Hunt[6] :

$$A_\alpha = 2M \tag{18}$$

and

$$A_\beta = 2M(1 - C_e)/C_e \tag{19}$$

where

$$M = \sum_{n=1}^{\infty} (J_1^2(1-C_e)^{1/2})/(J_0^2(n\pi)) \tag{20}$$

In equation 20, $J_0$ and $J_1$ are Bessel functions.

Our numerical results show that $\Delta$ is proportional to $\Lambda$ for a fixed $\Gamma$, or :

$$\Delta = \Lambda f(\Gamma) \qquad (21)$$

Following the procedure just described, in a previous work Chandrasekhar[8] developed a numerical model to calculate the average concentration over the solid phases. To reduce computational difficulties, he assumed that the rods have a square cross-section. Here we approximated circular rods by an array of small elements. We compared our results with Chandrasekhar's for $\Gamma = 0$ (no convection) and $\Lambda = 0.05$, as well Jackson and Hunt's analytical results for cylinders. For a composition of $C_e = 0.1$, the average concentration over the matrix ($\alpha$ phase) using the present model was calculated to be 0.10037, while the analytical solution produces $C_{i\alpha}^* = 0.10025$ and Chandrasekhar's analysis gave $C_{i\alpha}^* = 0.10049$. The corresponding values of the average composition over the rods ($\beta$ phase) are : $C_{i\beta}^* = 0.09667$ using the present model, $C_{i\beta}^* = 0.09775$ using the analytical solution and $C_{i\beta}^* = 0.09577$ in Chandrasekhar's work. It can be seen that the use of an array of small rectangular elements to represent the cross-sections of the rods, yields results closer to the analytical solution for circular cross sections. There are several factors which explain the deviation from the analytical results, but among them, the more important are probably :

i. The cross-sections of the rods were built using an array of discrete elements, while Jackson and Hunt[6] considered them as circles.

ii. Placing the rods on the corners of a hexagon rather than on a circle as done by Jackson and Hunt[6].

Following Baskaran and Wilcox[4], the spacing between the rods can be given by :

$$(\lambda/\lambda_0) = (1 - f/A - 2\Gamma/Adf/d\Gamma)^{-1/2} \qquad (22)$$

Figure 4 shows plots of f versus $\Gamma$. It is noted that the perturbation in the concentration field is bigger for a flow in the y direction. The distance between two rods represents an important parameter in the effect of the flow on the average composition over the $\alpha$ and $\beta$ phases. Since that distance is smaller in the x direction, the amount of solute over the matrix between two rods and available to be displaced by the convective flow, is smaller when compared to the corresponding distance in the y direction. Flow in the y direction displaces a larger amount of solute than an equivalent flow in the x direction, hence the average composition over the rods is more perturbed.

Also, as observed in figure 4, the effect of convection on the concentration field decreases with increasing eutectic composition. The perturbation in the concentration field due to convection, $\Delta$, is a function of two terms given by equation 14 and 15. During the numerical analysis, it was found that the change in the average composition over the rods ($\beta$ phase), is bigger than the change in average composition over the matrix ($\alpha$ phase). The sensitivity of $\Delta$ to eutectic composition decreases as this composition is increased.

Since f was calculated numerically using polynomial fits, $df/d\Gamma$ may easily be found by differentiating f with respect to $\Gamma$.

Substituting f and $df/d\Gamma$ in equation 22, $\lambda/\lambda_0$ was calculated as presented in figure 5. Polynomial fits of $\lambda/\lambda_0$ as a function of $\Gamma_0$ yielded :

For $C_e = 0.03$ and flow in the x direction :

$$\lambda/\lambda_0 = 1 + \Gamma_0 1.1 \times 10^{-3} + \Gamma_0^2 2.2 \times 10^{-7} - \Gamma_0^3 7.8 \times 10^{-9} \qquad (23)$$

For $C_e = 0.03$ and flow in the y direction :

$$\lambda/\lambda_0 = 1 + \Gamma_0 1.1 \times 10^{-3} + \Gamma_0^2 2.5 \times 10^{-6} - \Gamma_0^3 1.1 \times 10^{-8} \qquad (24)$$

For $C_e = 0.05$ and flow in the x direction :

$$\lambda/\lambda_0 = 1 + \Gamma_0 1.7 \times 10^{-3} + \Gamma_0^2 4.4 \times 10^{-6} - \Gamma_0^3 2.2 \times 10^{-8} \qquad (25)$$

For $C_e = 0.05$ and flow in the y direction :

$$\lambda/\lambda_0 = 1 + \Gamma_0 1.7 \times 10^{-3} + \Gamma_0^2 6.5 \times 10^{-6} - \Gamma_0^3 1.3 \times 10^{-8} \qquad (26)$$

For $C_e = 0.10$ and flow in the x direction :

$$\lambda/\lambda_0 = 1 + \Gamma_0 1.9 \times 10^{-3} + \Gamma_0^2 3.4 \times 10^{-6} - \Gamma_0^3 1.8 \times 10^{-8} \qquad (27)$$

For $C_e = 0.10$ and flow in the y direction :

$$\lambda/\lambda_0 = 1 + \Gamma_0 2.0 \times 10^{-3} + \Gamma_0^2 6.9 \times 10^{-6} - \Gamma_0^3 1.8 \times 10^{-8} \qquad (28)$$

The change in the undercooling with increasing convection was calculated using Chandrasekhar et al.'s equation[5], which is :

$$g(\Gamma_0) = (1 - f/A - 2\Gamma/Adf/d\Gamma)^{1/2} +$$
$$(1 - f/A)(1 - f/A - 2\Gamma/Adf/d\Gamma)^{-1/2} \qquad (29)$$

where A, f and $df/d\Gamma$ were obtained as before. Figure 6 shows $g(\Gamma_0)/2$ versus $\Gamma_0$.

An important motivation for this work was to estimate the effect of natural convection on spacing of rod eutectics. The value of $\Gamma_0$ computed for a typical experimental set-up[7] is $6.5 \times 10^{-3}$. For this value of $\Gamma_0$ and for the eutectic concentrations studied, $\lambda/\lambda_0 \approx 1$. Thus natural convection is not expected to change the spacing between the rods by perturbing the concentration field ahead of the growing eutectic interface.

## 4. CONCLUSION

Based upon the results obtained during this analysis, it can be affirmed that the spacings between the rods increase with an increase in convection. For the same intensity of convection, an increase in the

eutectic composition increases the rod spacing, but the change due to convection is smaller for higher eutectic compositions. Also, it was concluded that the direction of the convective flow plays an important role in changing the rod spacing, since a flow in the y direction provokes a bigger increase in the rod spacing than a flow in the x direction.

## ACKNOWLEDGEMENT

## NOMENCLATURE

$A_\alpha, A_\beta$ = Constants.

$C$ = Mass fraction of component A in the melt.

$C_e$ = Eutectic mass fraction.

$C_i$ = Interfacial melt composition.

$C_i^*$ = Average interfacial melt composition.

$C_\alpha$ = Composition of the $\alpha$ phase (the matrix, assumed 0.0 here).

$C_\beta$ = Composition of the $\beta$ phase (the rods, assumed 1.0 here)

$D$ = Diffusion Coefficient in the melt ($m^2/s$).

$f$ = $\Delta/\lambda$

$G_U$ = $\sqrt{G_{Ux}^2 + G_{Uy}^2}$ = $dU/dz$

$G_{Ux}$ = Gradient of transverse velocity in the x direction near the solid/liquid interface ($dU_x/dz$).

$G_{Uy}$ = Gradient of transverse velocity in the y direction near the solid/liquid interface ($dU_y/dz$).

$r_\alpha, r_\beta$ = Radius of the $\alpha$ and $\beta$ phases respectively (m)[6].

$U$ = Melt velocity parallel to the interface (m/s) = $\sqrt{U_x^2 + U_y^2}$

$U_x, U_y$ = Components of transverse velocity in the x and y directions

$V$ = Freezing Rate (m/s).

$x,y$ = Distances along the solid/liquid interface (m).

$X,Y$ = Dimensionless distances along the solid/liquid interface, $x/\lambda$ and $y/\lambda$.

$z$ = Distance into the melt from the interface (m).

$Z$ = Dimensionless distance into the melt from the interface, $z/\lambda$.

$\lambda_0$ = Value of $\lambda$ at $G_U$ = 0.

$\lambda$ = Spacing between the rods (m).

$\Gamma$ = $G_U\lambda^2/D$, Dimensionless convective velocity at the interface.

$\Gamma_x = G_{Ux}\lambda^2/D$, Dimensionless convective velocity at the interface in the x direction

$\Gamma_y = G_{Uy}\lambda^2/D$, Dimensionless convective velocity at the interface in the y direction

$\Lambda = \lambda V/D$ Freezing rate based Peclet number

**REFERENCES**

[1] R.G. Pirich and D.J. Larson, in: Materials Processing in Reduced Gravity Environment of Space, Ed. G.E. Rindone (North - Holland, New York, 1982) p. 523.

[2] R.G. Pirich, G. Bush, W. Poit and D.J. Larson, Jr., Met. Trans. 11A (1980) 193.

[3] G. Muller and P. Kyr, in: Proc. 15th European Symp. on Materials Science under Microgravity, Schloss Elmau, Nov. 1984, ESA SP-222, p.141.

[4] V. Baskaran and W.R. Wilcox, J. of Crystal Growth 67 (1984) 343.

[5] S. Chandrasekhar, G.F. Eisa and W.R. Wilcox, J. of Crystal Growth 78 (1986) 485.

[6] K.A. Jackson and J.D. Hunt, Trans. AIME 236 (1966) 1129.

[7] G.F. Eisa and W.R. Wilcox.: J. of Crystal Growth 78 (1986) 159.

[8] S. Chandrasekhar, PhD Thesis, Clarkson University, Potsdam (1987).

## LIST OF FIGURES

Figure 1. A rod eutectic structure viewed normal to the freezing inter-face. The smallest region satisfying the periodicity condition is shown by the rectangle. The arrows indicate the directions of the components of the convective velocity ($U_x$, $U_y$).

Figure 2. The three dimensional domain modelled. The crystallization flow V is parallel to the z-axis and the components of the convective flow are parallel to the x-axis and y-axis.

Figure 3.a. Three dimensional plot of concentration in the melt at the solid/liquid interface of the eutectic growing without convection, for $C_e = 0.03$, $\Gamma_x = 0$, $\Gamma_y = 0$ and $\Lambda = 0.05$.

Figure 3.b. Three dimensional plot of concentration in the melt at the solid/liquid interface of the eutectic growing with convection, for $C_e = 0.03$, $\Gamma_x = 280$, $\Gamma_y = 0$ and $\Lambda = 0.05$.

Figure 3.c. Three dimensional plot of concentration in the melt at the solid/liquid interface of the eutectic growing with convection, for $C_e = 0.03$, $\Gamma_x = 0$, $\Gamma_y = 280$ and $\Lambda = 0.05$.

Figure 4.a. The ratio of the perturbation in interfacial concentration, $\Delta$, to the rod spacing based Peclet number versus $\Gamma$, for convection in the x direction.

Figure 4.b. The ratio of the perturbation in interfacial concentration, $\Delta$, to the rod spacing based Peclet number versus $\Gamma$, for convection in the y direction.

Figure 5.a. The ratio of the rod spacing with convection in the x direction to that without convection, $\lambda/\lambda_0$, versus $\Gamma_0 = \Gamma/(\lambda/\lambda_0)^2$.

Figure 5.b. The ratio of the rod spacing with convection in the y direction to that without convection, $\lambda/\lambda_0$, versus $\Gamma_0 = \Gamma/(\lambda/\lambda_0)^2$.

Figure 6.a. The ratio of minimum undercooling with convection in the x direction to that without convection, $g/2$, versus $\Gamma_0 = \Gamma/(\lambda/\lambda_0)^2$.

Figure 6.b. The ratio of minimum undercooling with convection in the y direction to that without convection, $g/2$, versus $\Gamma_0 = \Gamma/(\lambda/\lambda_0)^2$.
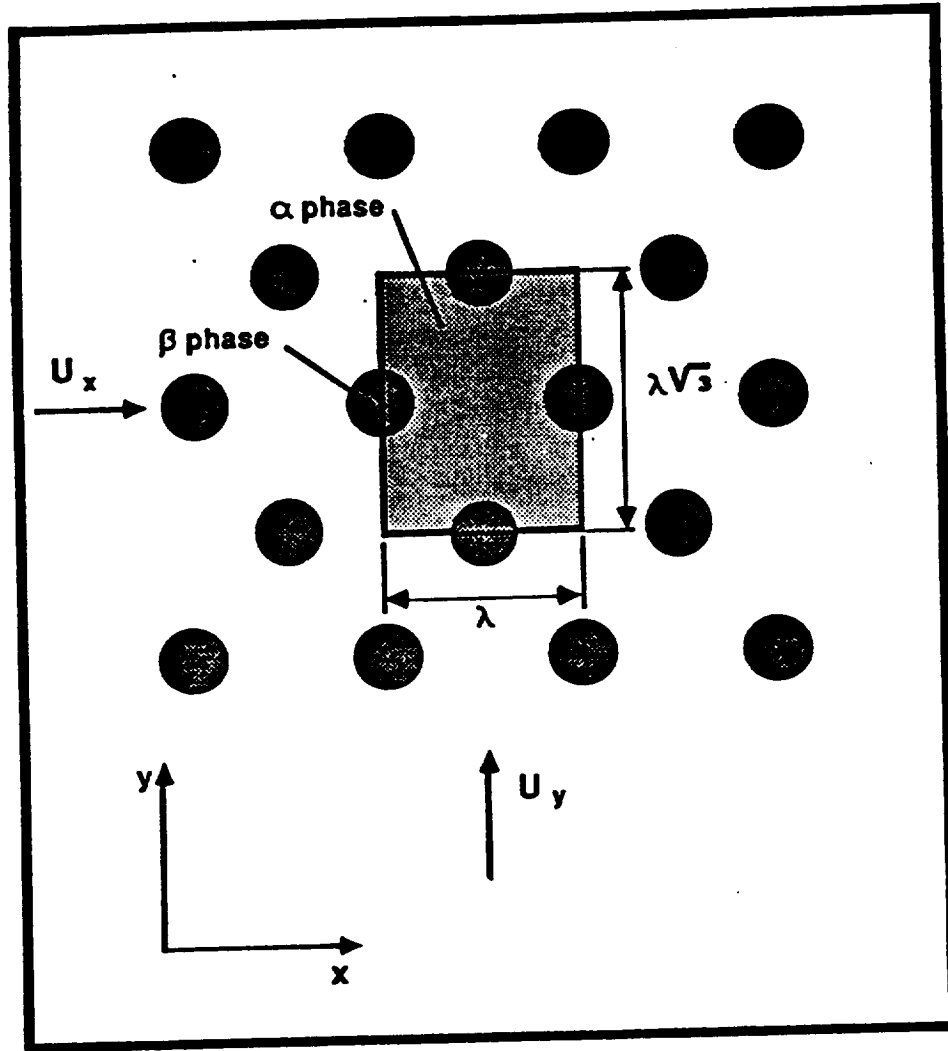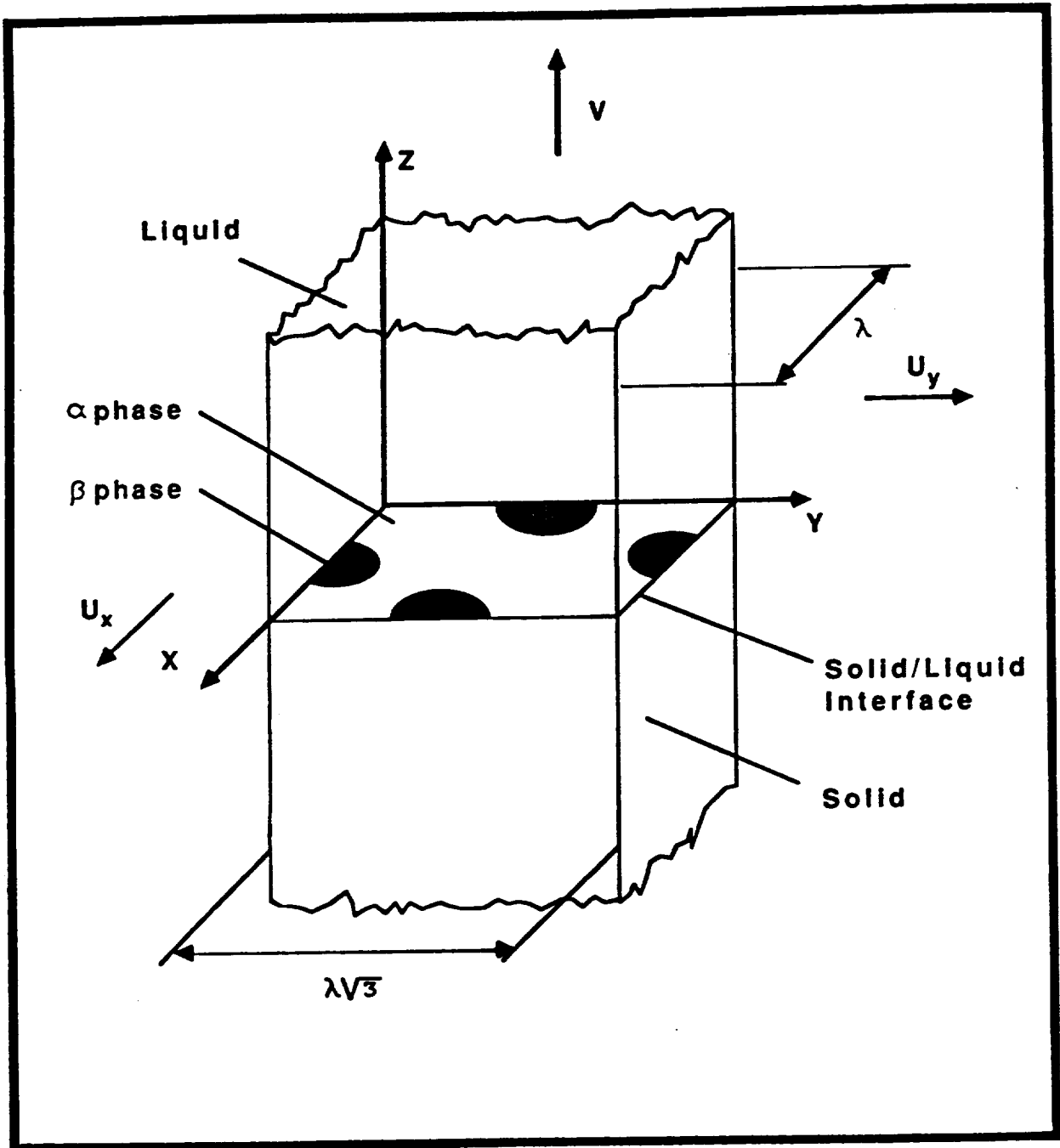
Figure 1

**Figure 2**

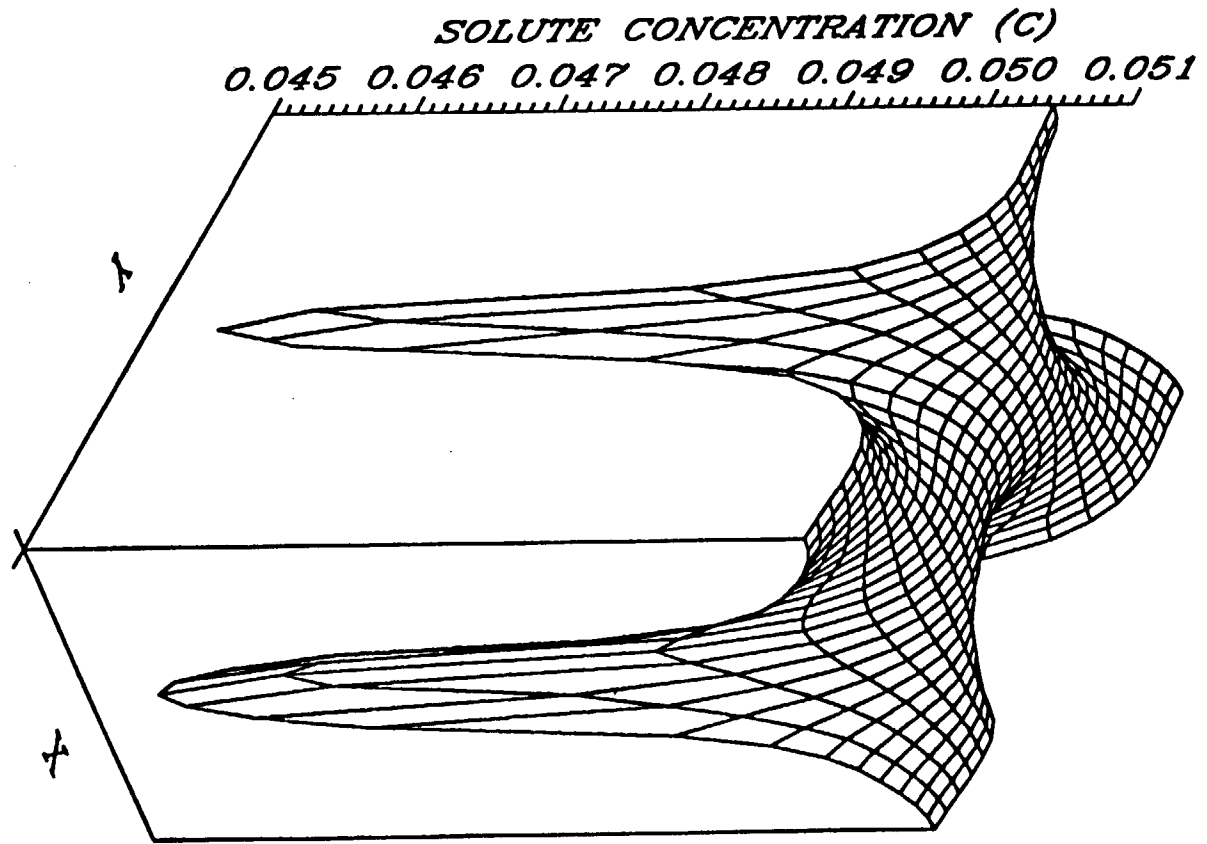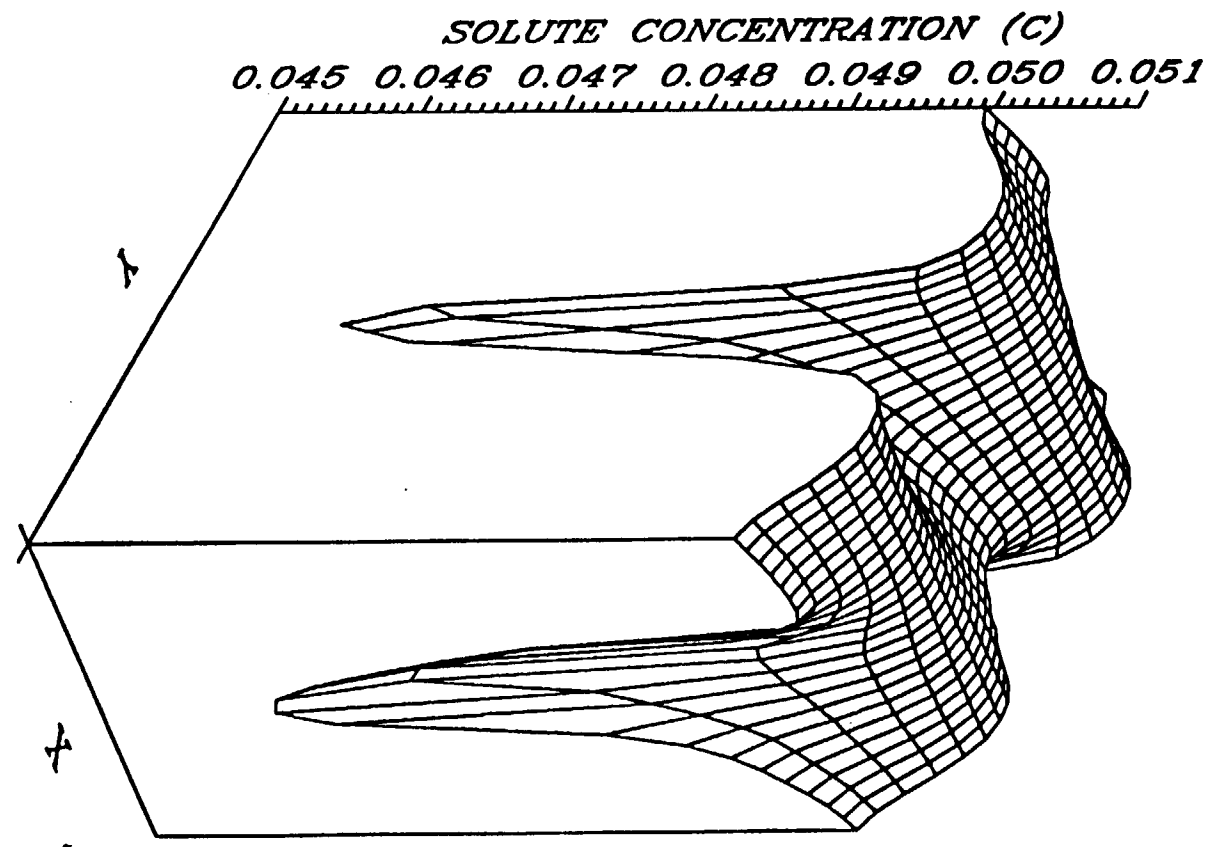SOLUTE CONCENTRATION (C)

0.045  0.046  0.047  0.048  0.049  0.050  0.051

Figure 3.a

SOLUTE CONCENTRATION (C)

0.045 0.046 0.047 0.048 0.049 0.050 0.051

Figure 3.b

SOLUTE CONCENTRATION (C)
0.045  0.046  0.047  0.048  0.049  0.050  0.051

Figure 3.c

Figure 4.a

Flow x−direction — Ce=0.03
Flow x−direction — Ce=0.05
Flow x−direction — Ce=0.10
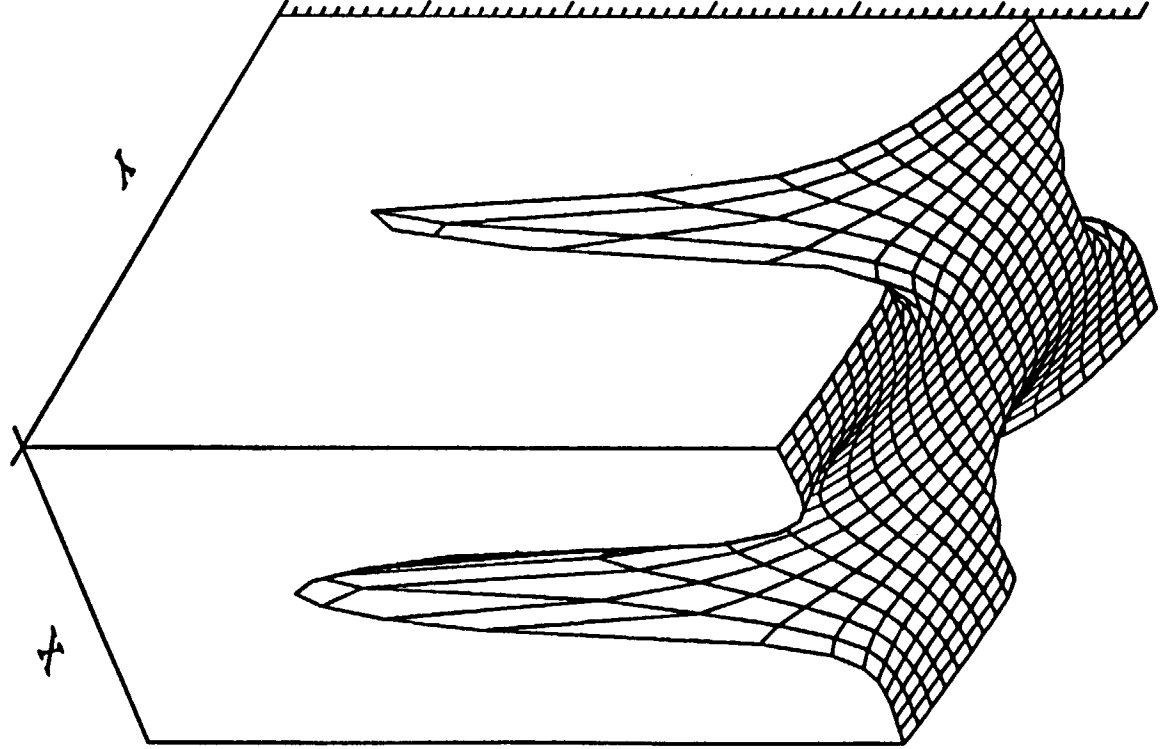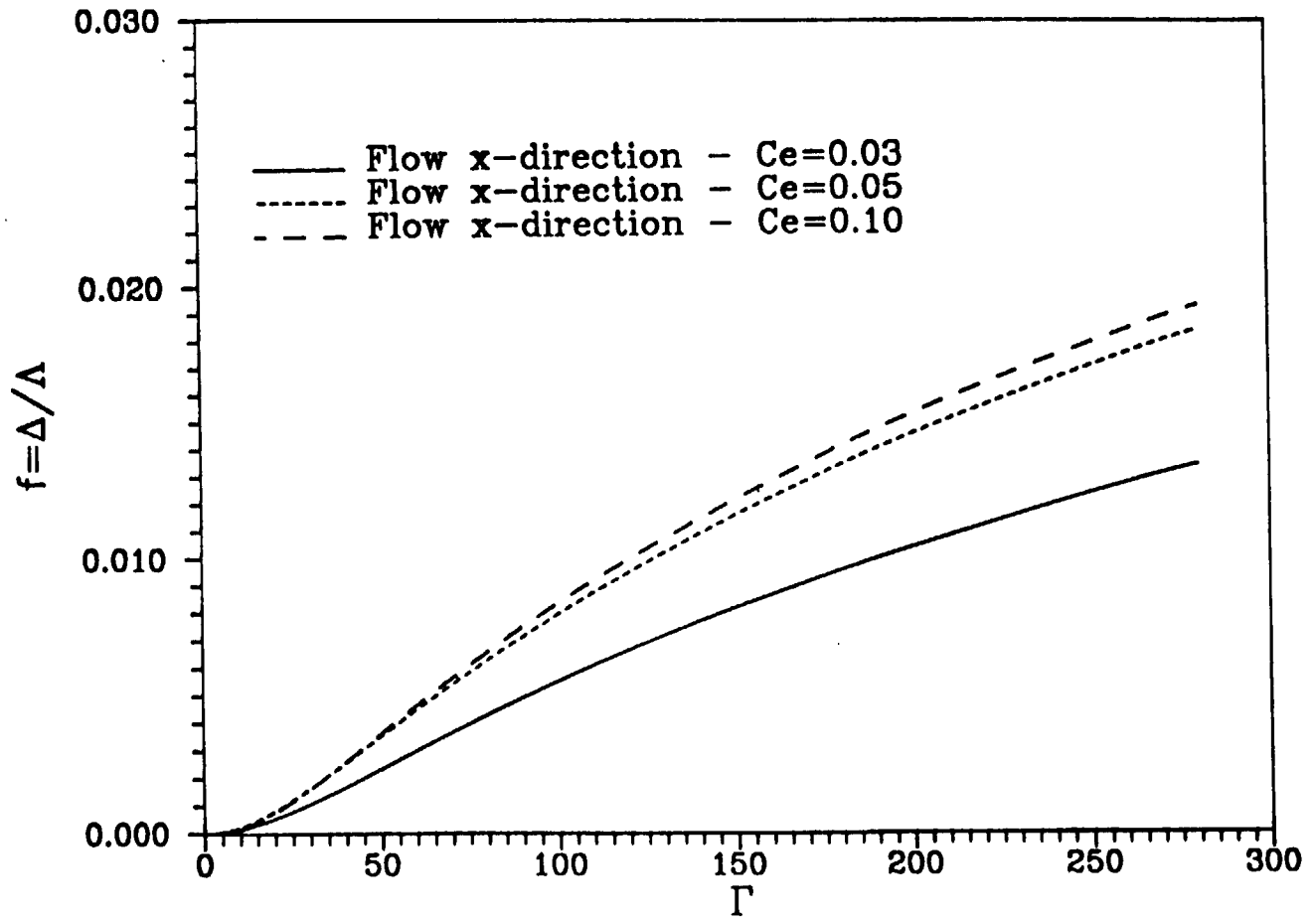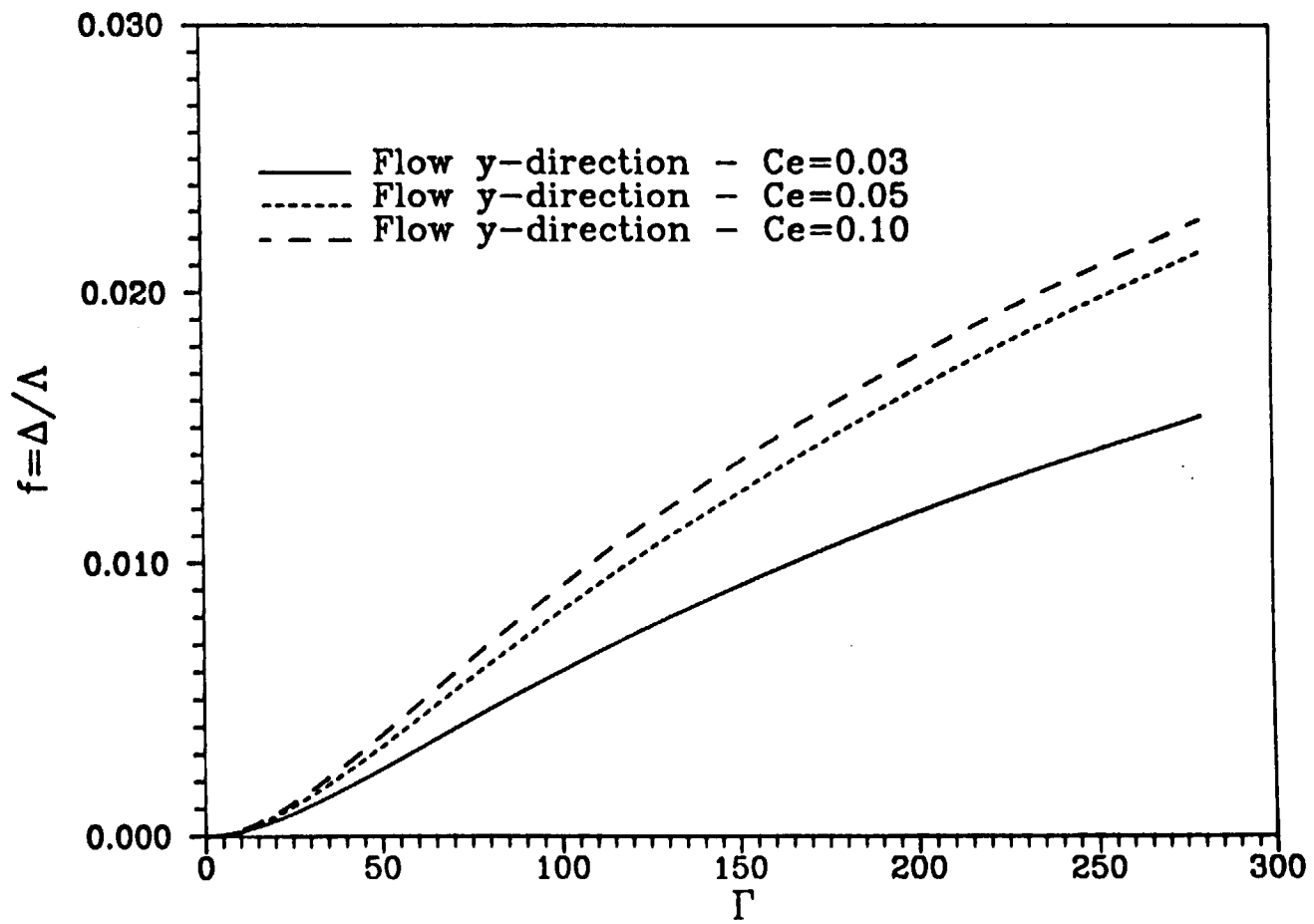
Figure 4.b

Figure 5.a
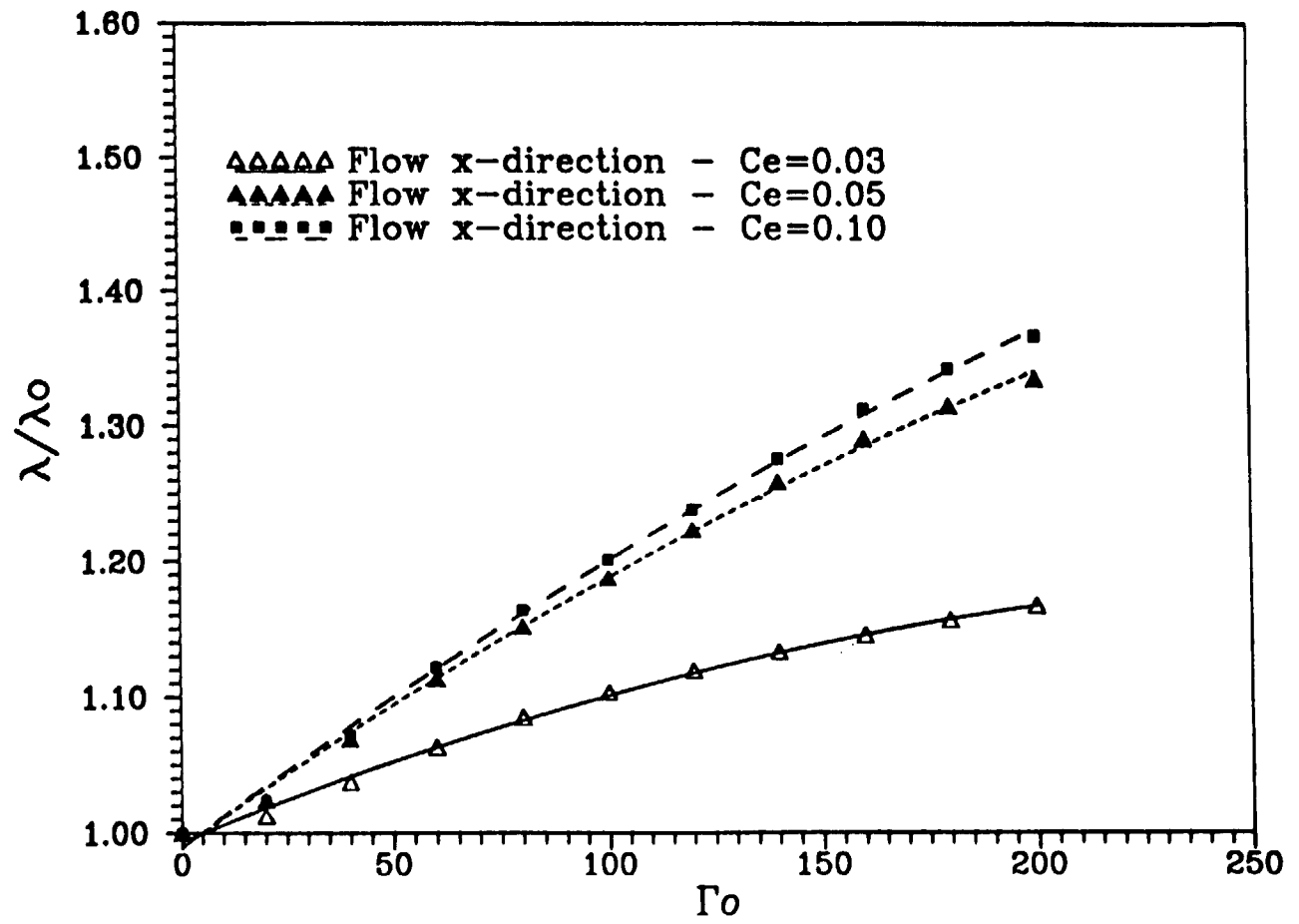
# II   EXPERIMENTAL DETERMINATION OF THE SORET COEFFICIENT OF Mn-Bi MELTS

A. P. Mohanty and R. Caram

## Summary

The objective of this project was to determine the Soret coefficient in eutectic Mn-Bi melts. We attempted to determine the Soret coefficient (thermal diffusion coefficient) of Mn-Bi melts experimentally. The experimental apparatus was built and a number of experiments conducted. The samples from the experimental runs were analysed and concentration profiles obtained. The profiles were compared to theoretically determined profiles. Preliminary calculations show that the Soret coefficient is in the range of $1 \times 10^{-7}$ cm$^2$/s°C and $1 \times 10^{-8}$ cm$^2$/s°C.

## A. Introduction

The growth of eutectic and eutectoid structures has received considerable theoretical and experimental attention because these fine periodic microstructures often show improved mechanical properties [1-7]. Eutectic or near eutectic alloys can be directionally solidified to obtain *in-situ* composite structures.

The interest in the work done here at Clarkson [8-13] was created by the observed change in the microstructure of MnBi-Bi alloys caused by solidification in space. It was found that the fiber spacing of the space processed sample was about half the spacing of the same material when solidified on earth under otherwise identical conditions. The observation held over a wide range of freezing rates. The absence of natural convection in space is considered to be one of the main reasons for the above results. The actual mechanism by which convection affects the fiber spacing has not yet been determined. Similar experiments have been conducted by other investigators on other eutectic melts leading to a wide variety of results.

Thus far the work done has not led to an explanation of the reduction in MnBi fiber spacing for a space grown sample compared to that grown on earth. Theoretical work at Clarkson led to the prediction that convection during solidification coarsens an eutectic microstructure by altering the concentration field in front of the freezing interface. The theoretical predictions agreed well with experiments using vigorous convection caused by spin-up/ spin-down (accelerated crucible rotation technique). However little effect of buoyancy driven convection was predicted, so that the theory provided no explanation for the space results. The theoretical treatment assumed a planar interface, no Soret effect (thermal diffusion), melt composition precisely at the eutectic, equal volumetric properties in all three phases, and rapid interface kinetics. Violation of one or more of these assumptions, as occurs for real eutectic solidification, might make the microstructure much more sensitive to convection.The purpose of the present project was to determine the Soret coefficient and diffusion coefficient of the MnBi melt. A theoretical model was made and the results compared to the experimentally obtained concentration profiles. The experimental method

adopted in this project involved the experimental determination of the temperature gradient and the concentration gradient.

When a fluid is held in a temperature gradient in the absence of convection, the components slowly separate. This is called thermal diffusion for fluids in general and the Soret effect for liquids. The determination of the Soret coefficient is if the compositional gradients are known. In the absence of any reliable values, the molecular diffusion coefficient and the Soret coefficient are determined simultaneously. The experimental method requires the determination of the temperature gradient, the concentration gradient and concentration versus time.

## B. Progress

Given below are the details of the equipment, the experiment and the analysis of the samples. It was necessary to obtain a convection free environment. Hence the first step was to design the appropriate equipment. Also it was desirable to be able to keep a linear temperature profile. A detailed description of the apparatus and the experimental procedure is given in the following pages.

## 1. Apparatus

An important part of the project was the design of the apparatus. Many different options were considered. A schematic of the final apparatus is shown in figure 2.1. The apparatus can be divided into three main sections:

- The furnace
- The ampoule
- The temperature control unit

### a. Furnace

The core of the furnace consisted of a metal rod with a 5mm hole drilled through it. The diameter of the rod was 0.5 inch (1.27 cm). The rod was to be thick enough so that there was a good chance of obtaining a linear temperature profile. The limiting factor on the diameter of the rod was the machinability of the metal. Initially a brass rod was used, but after a few runs the brass oxidized and there was some reaction between the quartz and the brass. In figure 2.2 there are some pictures showing the oxidized brass. To avoid oxidation, a stainless steel rod (AISI type 446) was used and worked well. The gap between the ampoule wall and the inner wall of the furnace had to be as small as possible, so as to reduce air drafts. The ampoule was expected to be 3mm in outer diameter. Thus the furnace being 5mm ID gave some room for changes in ampoule diameter and for it not to be perfectly straight.

The furnace was positioned vertically and had two heaters at the ends. The two ends of the rod were machined down so that a quartz tube could slide over the ends.
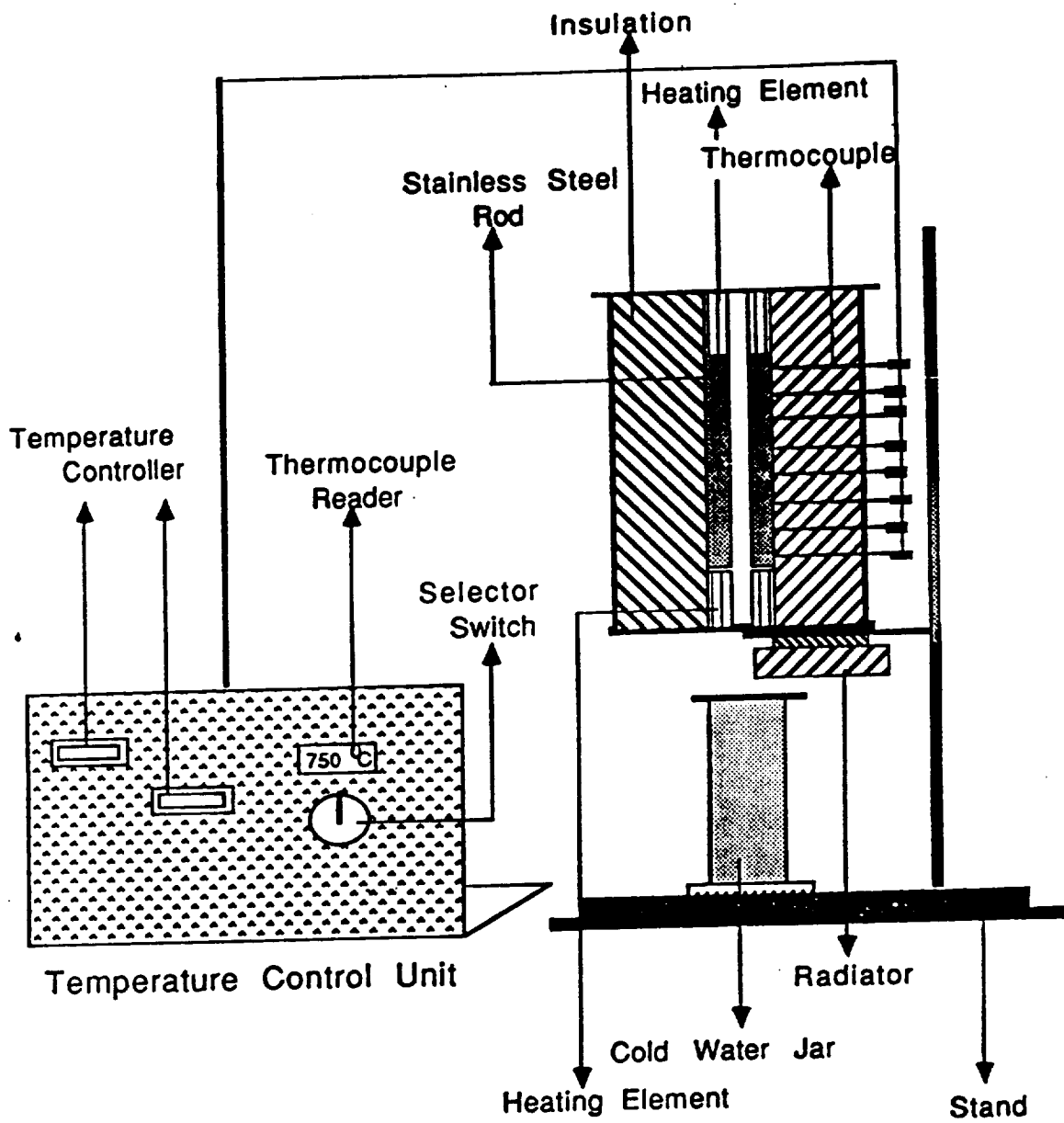
Figure 2.1: Schematic diagram of the apparatus used for the experiments.

Figure 2.3 shows the heater. The heater consists of a Kanthal wire wound on the quartz tube. The top heater was maintained at a higher temperature than the bottom heater. To ensure that the heater resistance wire coils did not touch each other, the heater element was protected with porcelain fish spine (Omega engineering, Inc.).

Furnace characteristics:
Hot zone:
Input voltage: 8 volts
Temperature:700 ° C
Heater electrical resistance: $5\Omega$

Cold zone:
Input voltage:4 volts
Temperature: 400 ° C
Heater electrical resistance:$5\Omega$

The whole furnace was mounted on a stand. The bottom end of the furnace was kept closed with a flat piece of metal. The metal piece at the bottom of the furnace was not fixed and could be easily removed. Below the furnace is a cylindrical jar with ice water. At the end of an experiment the metal piece was pulled out and the ampoule containing the material slipped down into the jar of ice water and was quenched. The whole furnace is well insulated with three layers of an alumina based ceramic fiber insulation (Cotronics corporation). Each layer of insulation is about 0.5 cm thick. Some pictures of the furnace are shown in the following pages.

## b. Ampoule

The ampoule was designed to limit the convection in the melt to a minimum. As mentioned before, convection is governed by the Grashof number. One way of keeping the Grashof number and hence the convection low is to have a small diameter. After loading the material the ampoule is sealed under vacuum. The cleaning and loading procedure is described later in this chapter. The vacuum and the small diameter of the ampoule create an effect such that the melt rises upwards inside the ampoule when it is heated in the furnace. The smaller the diameter the more difficult it was to work with. Considering the above factors, an inner ampoule diameter of 1mm was reasonable.

The outer diameter of the top end of the ampoule had to be 11 mm because it was the smallest diameter that the vacuum system in the laboratory could handle. The bottom end of the ampoule had to be open because it was not possible to force any kind of liquid into the thinner part of the ampoule with one end closed. A quartz ampoule is shown in figure 2.4. Quartz was preferred over other materials because of the extended period of the experiment and the temperature range. The upper limit of temperature in the experiment is 800 ° C and quartz fuses at about 1400 ° C.

(a)



(b)

Figure 2.2: Top: The oxidized brass furnace fused with the quartz at the hot end of the furnace. Bottom: The middle section of the brass furnace after it oxidized. The maximum temperature at the hot end did not exceed 750 ° C at any time during the running of the furnace.
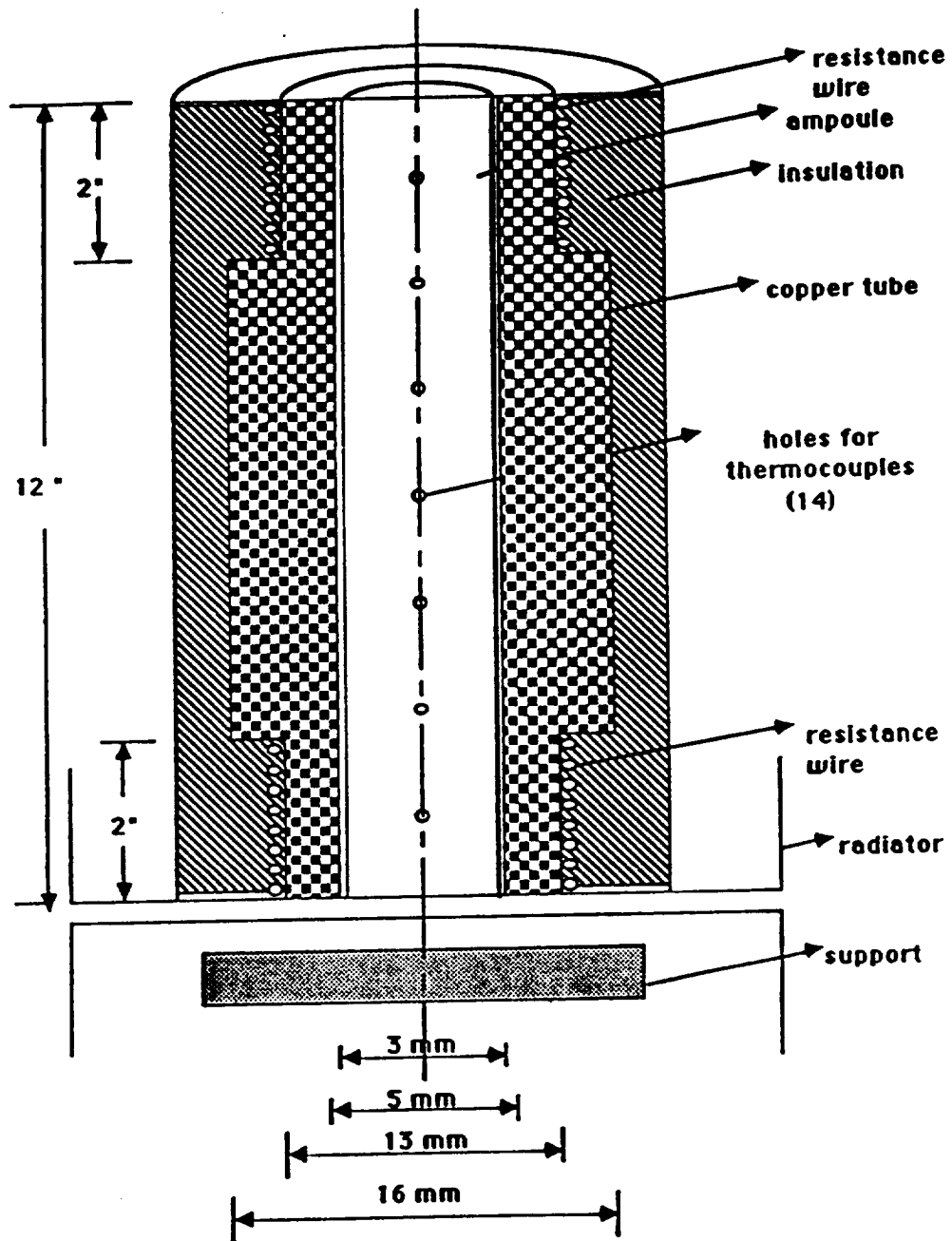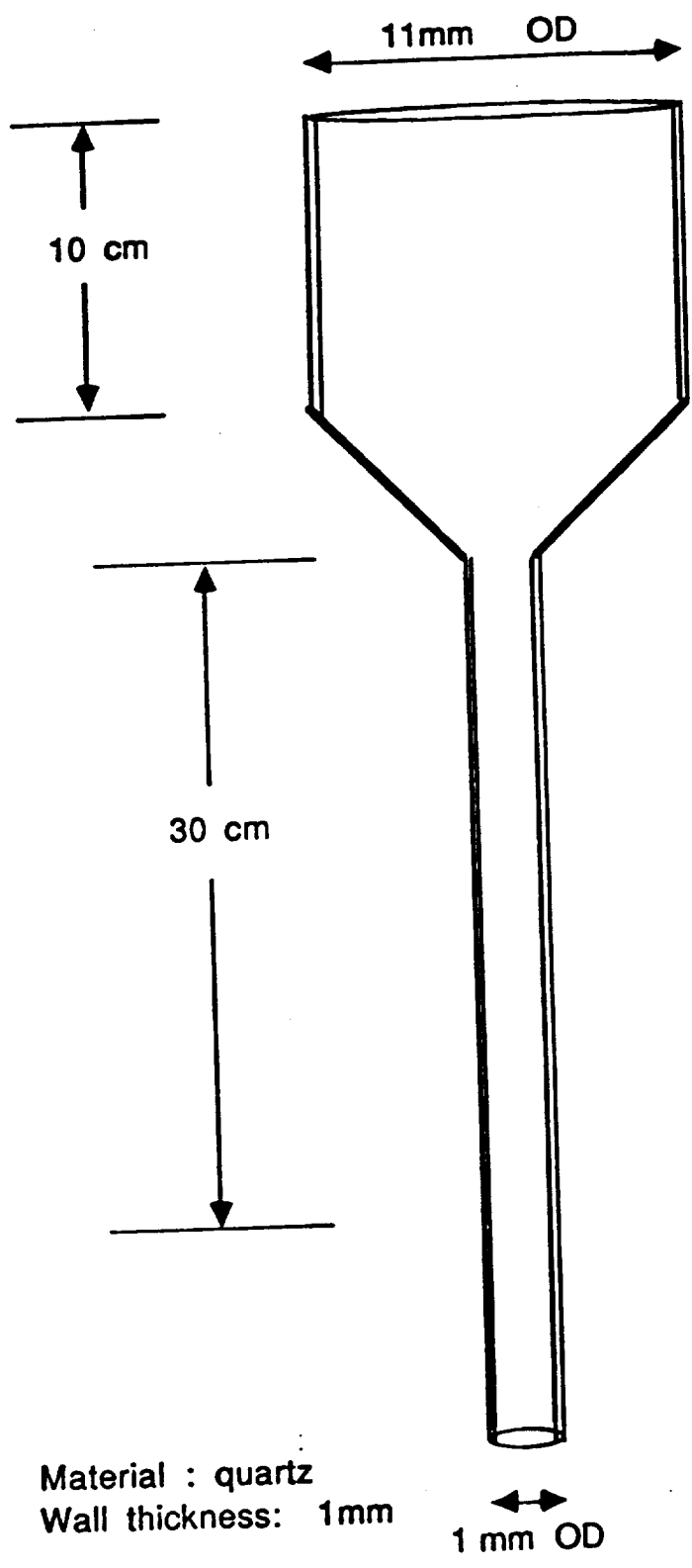
Figure 2.3: Longitudinal cross-section of the furnace showing the two heaters and the holes for the thermocouples along the length of the furnace.

11mm OD

10 cm

30 cm

Material : quartz
Wall thickness: 1mm

1 mm OD

Figure 2.4: Design of the ampoule used to load the material in the furnace. The broad part of the ampoule is cut off after sealing the ampoule.

### c. Temperature Control Unit

The temperature was measured along the length of the furnace with type K thermocouples. Small holes were drilled at regular intervals of 1.6 mm and the thermocouples were introduced through these such that they touched the ampoule wall. To read the temperature, the thermocouples are connected to a digital thermocouple reader (Omega engineering, Inc.) through a selector switch. The thermocouples in the heaters were connected to the temperature controllers (Eurotherm Corporation).

The temperatures in the two heaters were controlled by two separate controllers. The current and voltage could be varied with the two Variacs in the control unit. The temperature was displayed by the digital thermometer on the panel. All the thermocouples were connected to the display through a selector switch. There was also a fuse box and a number of electrical output sockets on the control unit. The whole unit was mounted on wood.

The furnace temperature profile could be approximated with a linear fit. But a second degree polynomial fit the data more closely. A typical profile is shown in figure 2.5. The polynomial fit is shown in figure 2.8 and figure 2.9. The temperature gradient for the stainless steel furnace was 23 ° C/cm. The temperature profile of the furnace was also calculated analytically using a fin equation to approximate the system. The theoretical temperature profile was similar to the experimentally obtained profile. The temperature profile obtained by theoretical calculation is shown in figure 2.7.

## 2. Experimental Procedure

The experimental procedure was a series of processes:

- Material preparation
- Ampoule preparation
- Experiment
- Analysis

### a. Material Preparation

Eutectic MnBi-Bi were solidified from 99.9999 % Bi (Johnson Matthey Inc.) and 99.99 % Mn (Aldrich Chemical Company Inc.). The MnBi-Bi eutectic composition is 0.71 ± 0.03 wt % Mn [21]. A balance with an accuracy of 0.1 mg was used to weigh 49.645 grams of Bi and 0.355 grams of Mn. The weighed Mn and Bi were loaded into a cleaned quartz ampoule and sealed under vacuum. The cleaning procedure is explained in the next section.

The material was homogenized in a rocking furnace. The temperature of the
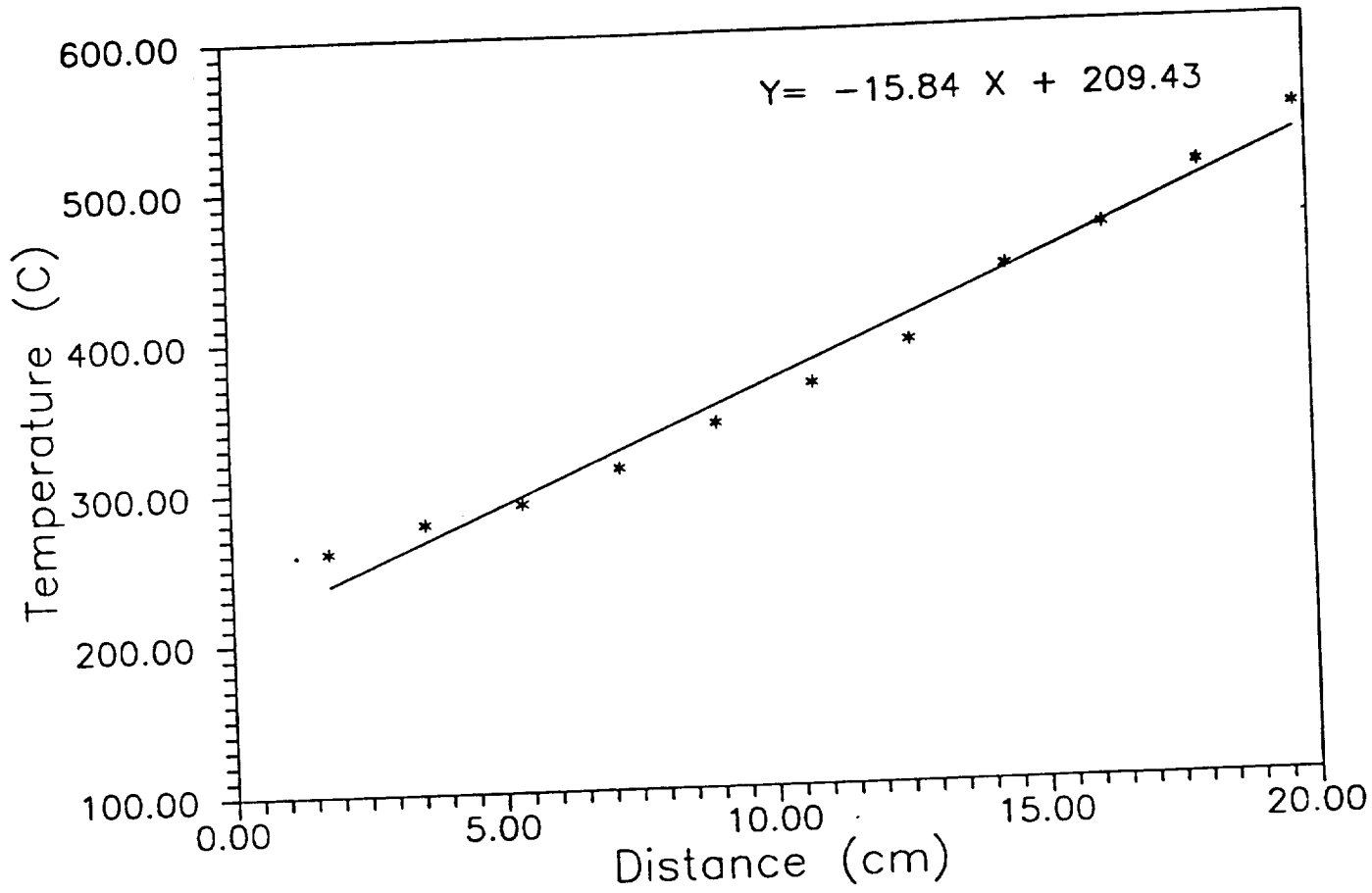
Figure 2.5: Experimentally determined temperature profile of the diffusion furnace with a brass core.
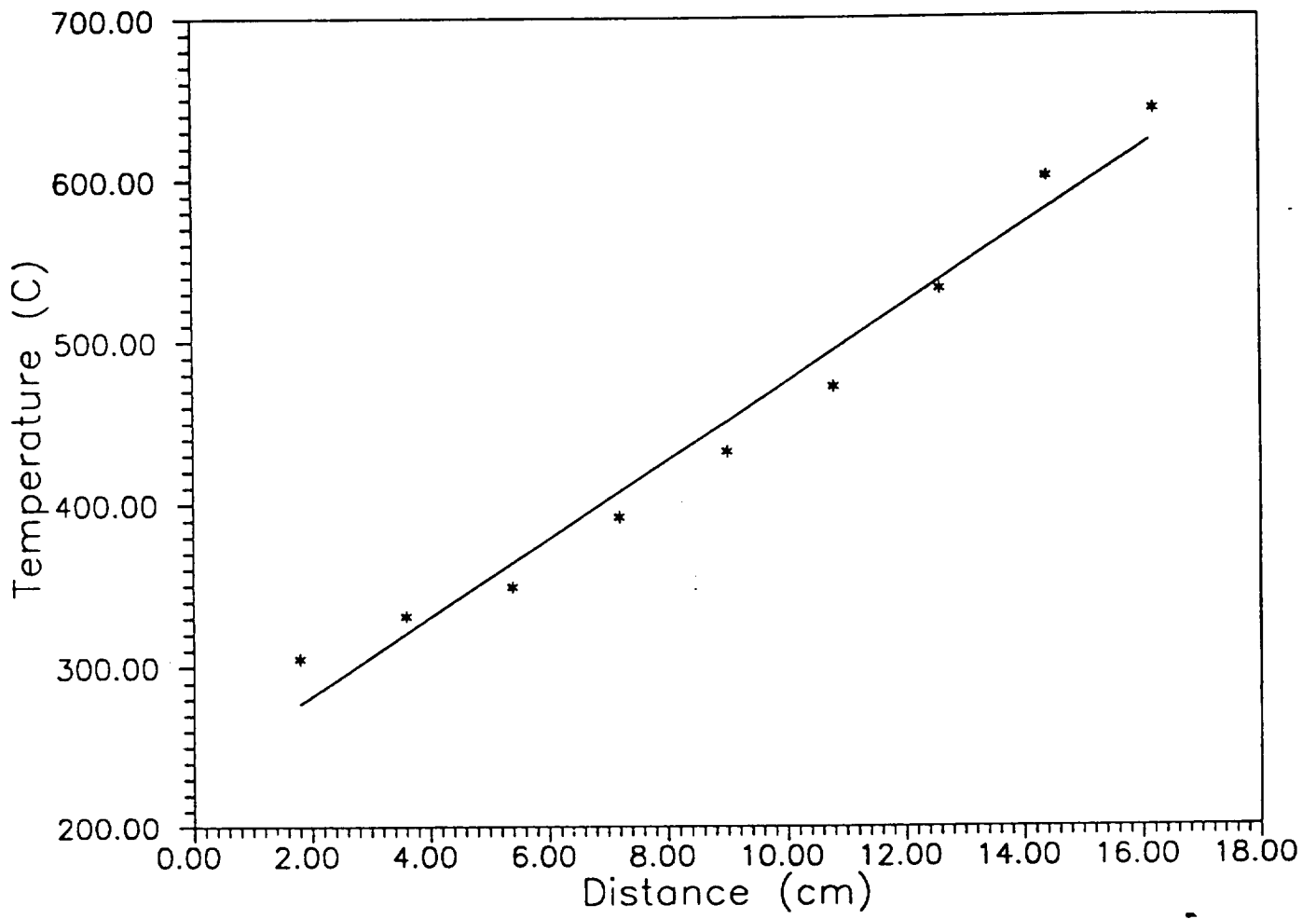
Figure 2.6: Experimentally determined temperature profile of the diffusion furnace with a stainless steel core.
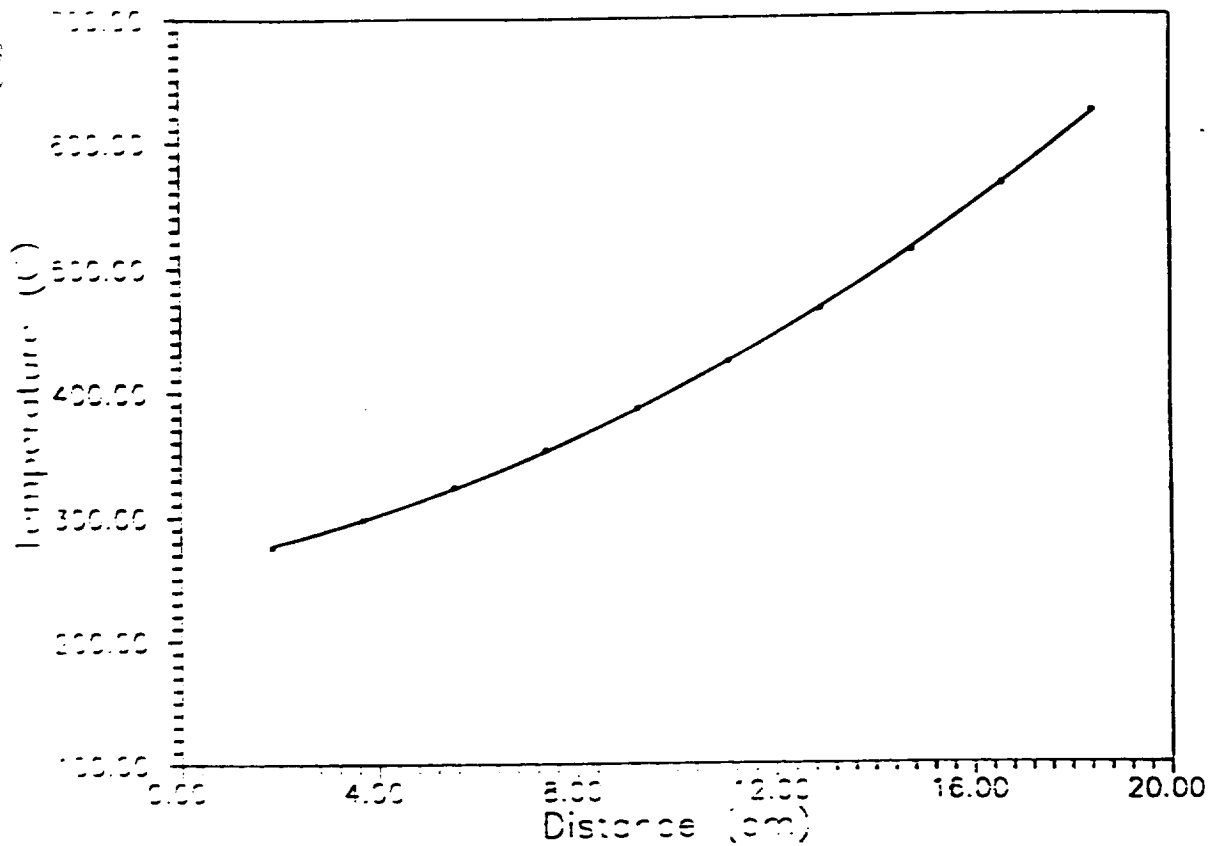
Figure 2.7: Temperature profile of the diffusion furnace obtained by theoretical calculation (curve obtained by using a second order polynomial fit).

furnace was maintained at 650 ° C. The temperature of the rocking furnace was increased in steps of 30. The material was left in the furnace for 24 hours with alternate periods of rocking and no rocking. The furnace was then slowly cooled down. The Mn-Bi was extracted from the ampoule by dissolving the quartz ampoule in HF. The extracted solid eutectic was etched with acetic acid and treated with acetone to remove any oxide layers. To test for homogeneity, samples of the material were taken and differential thermal analyses (DTA) were performed. All the samples had the same melting point, the eutectic melting point. The output graphs from the DTA are shown in figure 2.10 and figure 2.11. The solidified eutectic was ground to a powder with a clean mortar and pestle.

## b. Ampoule preparation

As explained in the section on ampoule design, the tip of the ampoule had to be open because of the difficulty in getting the cleaning agents into the ampoule. The cleaning procedure involved allowing the fluids to run through the ampoule. First the ampoule was cleaned with Micro solution, a laboratory cleaner with the following ingredients: cations - sodium, ammonium, triethanolammonium; anions - ethylenediaminetetraacetate, linear alkyl sulfonates; nonions - polyethoxynonylphenol, water; manufactured by International Products Corporation. This was followed by running the following through the ampoule: methanol, trichloroethane, acetone, methanol, HF and aqua regia respectively. The ampoule was rinsed with deionized water after each chemical was run through it. A squirt bottle was used for forced rinsing. The ampoule was then fixed upside-down in a clamp and allowed to dry at room temperature. One end of the ampoule was then sealed with a blow torch. The powdered Mn-Bi is loaded into the ampoule. The loaded ampoule is evacuated. The material is allowed to sit in the vacuum for a few hours. The ampoule is backfilled with
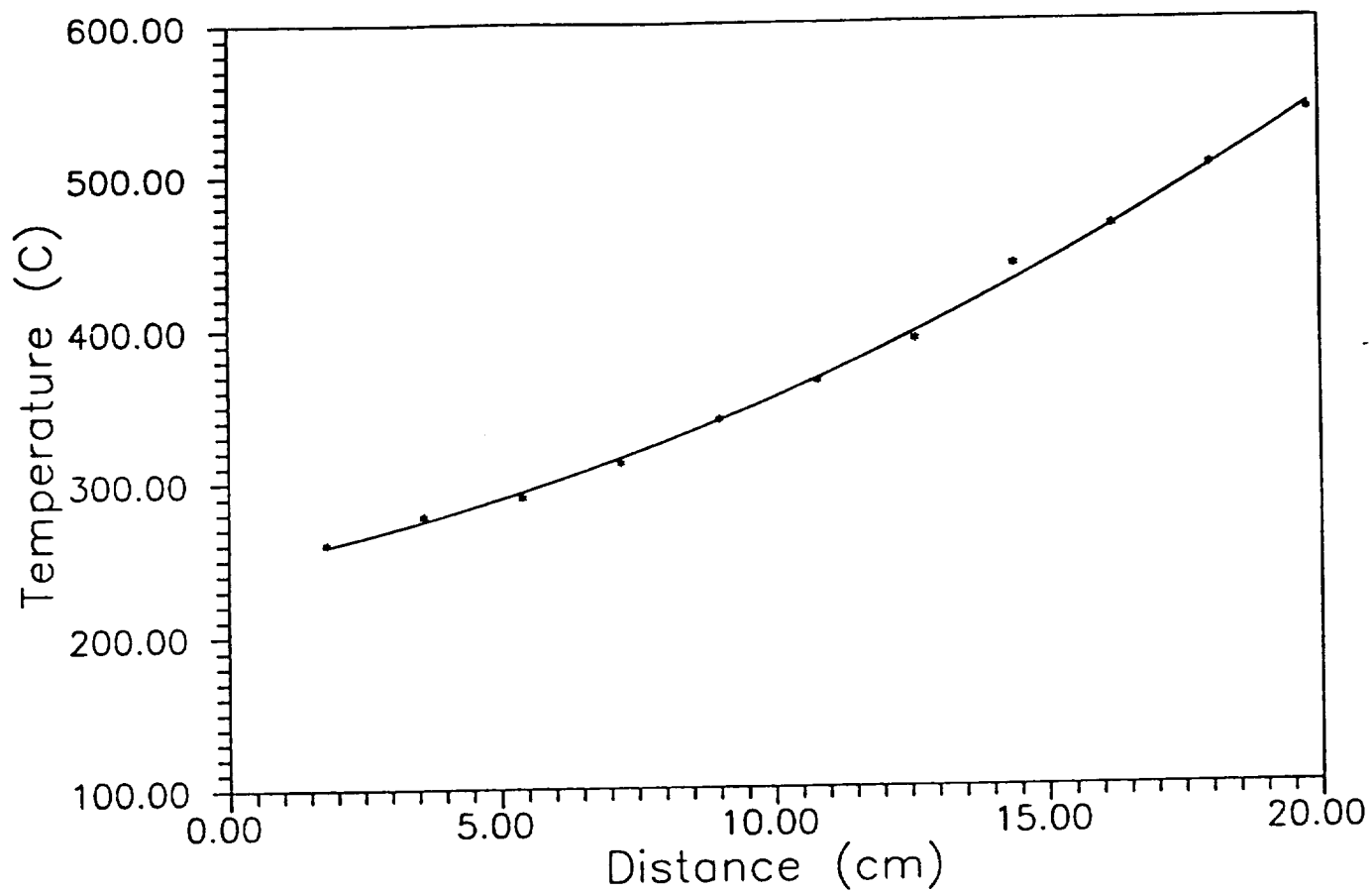
Figure 2.8: Experimentally determined temperature profile of the furnace obtained by fitting a second order polynomial
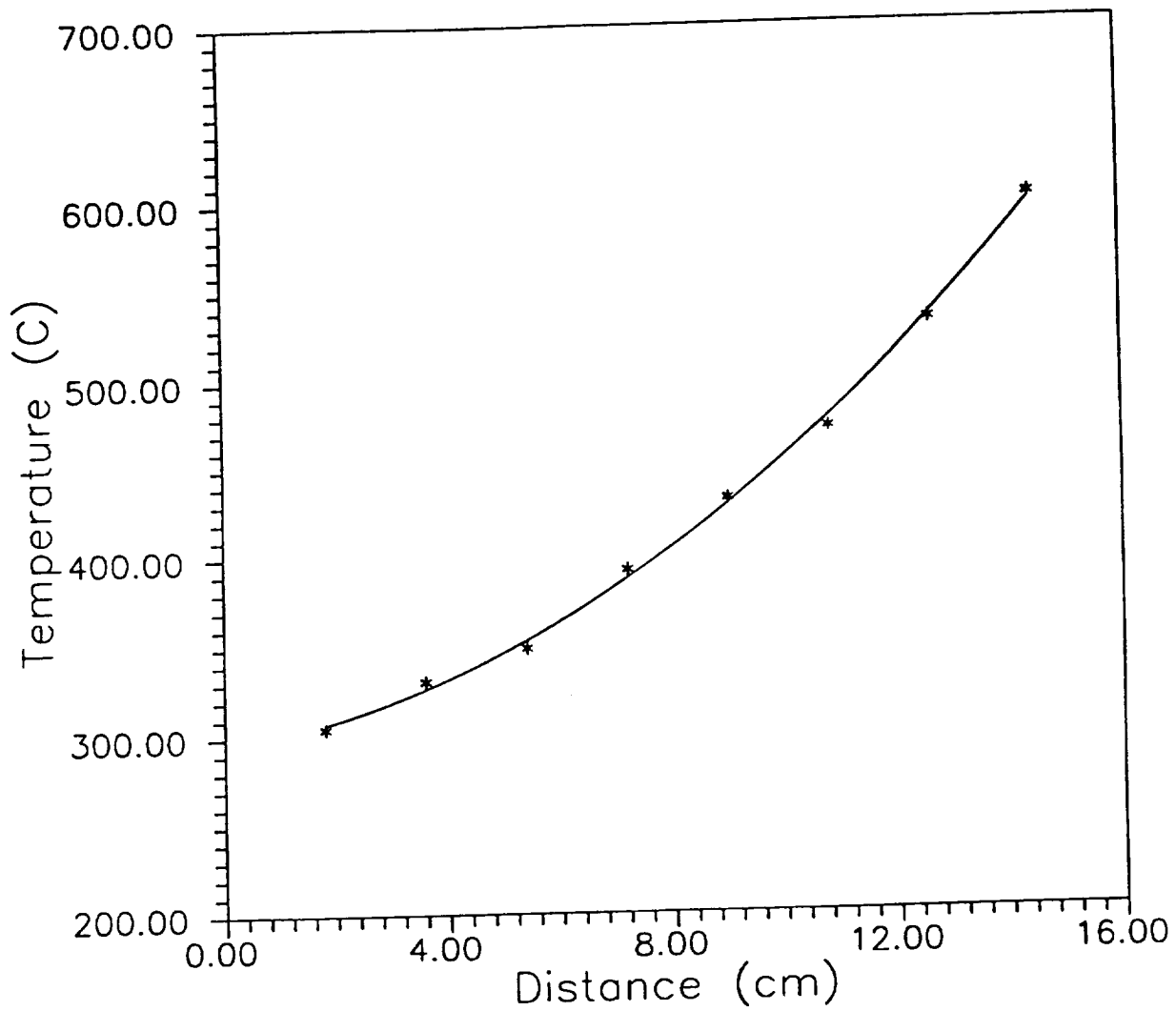
Figure 2.9: Experimentally determined temperature profile of the furnace with a stainless steel core obtained by fitting a second order polynomial.
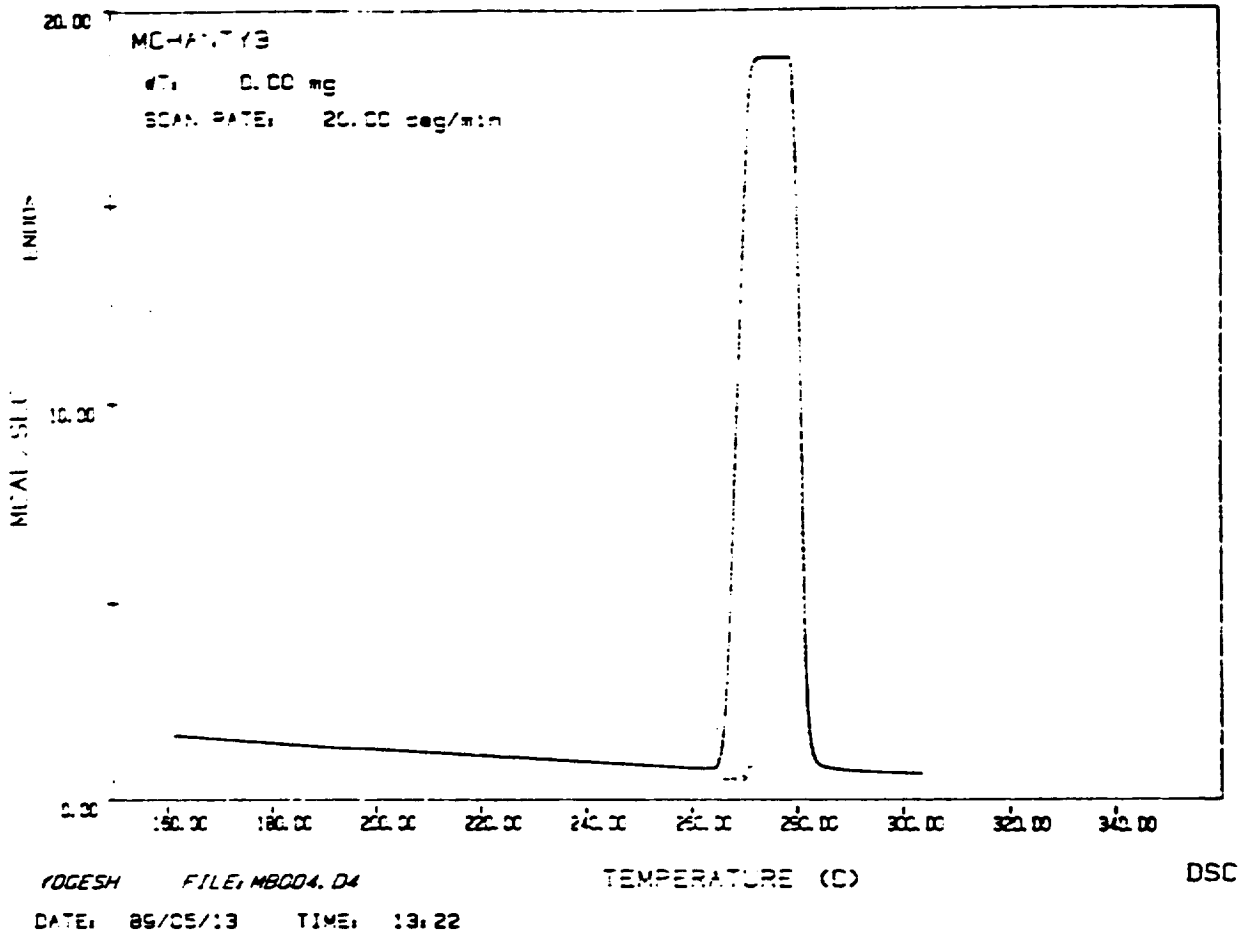
Figure 2.10: Differential thermal analysis of solidified Mn-Bi eutectic. The beginning of the peak is the melting point.
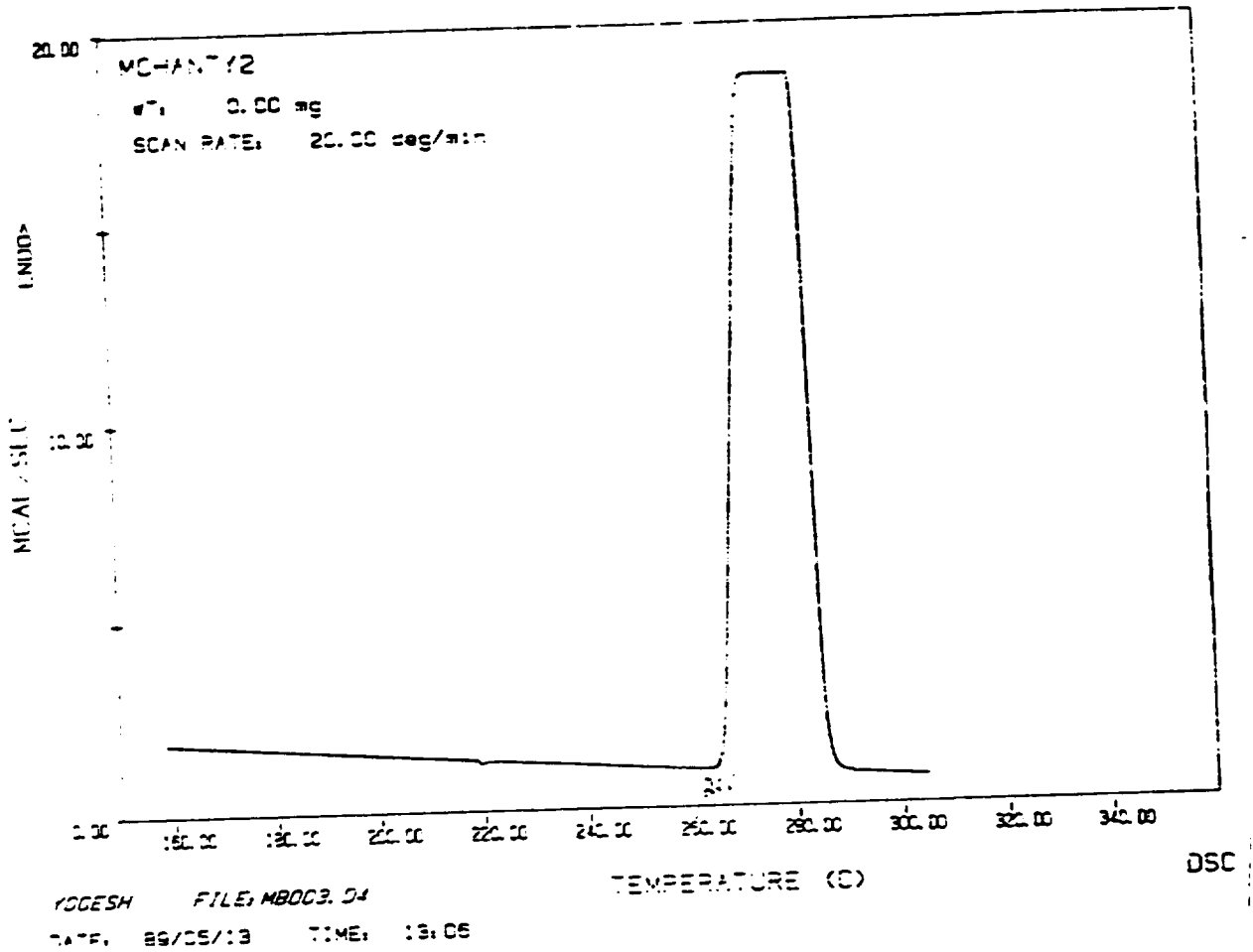
Figure 2.11: Differential thermal analysis of another Mn-Bi sample. The beginning of the peak is the melting point.

argon and flushed 2-3 times before sealing with a blow torch. Initially it was difficult to obtain good compacting of the material. On solidification the sample showed bubbles or gaps. To prevent the formation of gaps the sample was melted in steps, each time pulling the ampoule out of the furnace and gently tapping to compact the material.

## c. Experiment

The furnace was allowed to attain a steady temperature profile. The hot end of the furnace was maintained at 700 or 750 $^\circ$ C and the cold end was kept at 300 $^\circ$ C. The prepared ampoule was left in the furnace for a set time. The ampoule is quenched by dropping it into a jar of cold water. The crystal was extracted by etching the quartz away with HF. The sample was analysed by atomic absorption spectroscopy, as described below.

# 3. Analysis

The quenched sample was cut into small pieces of measured length. A map of the sample was made so as to be able to locate the position of each piece. Each piece was weighed and dissolved in a standardized volume of 10 % nitric acid. Atomic absorption spectroscopy (AA) was done to determine the amount of Mn in the sample. The AA machine used was the Perkin-Elmer model 5000. A schematic of the machine is shown in figure 2.12. The Perkin Elmer Zeeman 5000 is a microprocessor-controlled atomic absorption spectrophotometer. All the mechanical, electrical and optical functions of the instrument are electronically controlled and activated, enabling the analytical conditions to be set either manually via the keyboard, or from preprogrammed magnetic cards. Analytical conditions are entered using keyboards. Each control parameter has a separate key, which is used to assemble the analysis program. The completed program can be saved and recalled later. Recalling a program automatically resets the instrument parameters to the desired values.

A number of publications give a general background on the principles of operating an atomic absorption instrument [14,15]. The Perkin Elmer manual lists a number of analytical techniques. The conditions and parameters used for our analysis were taken from the manual. In all the analyses, the flame aspirator with the impact bead flow modifier was employed. Manganese lamp for the Zeeman 5000 was purchased from Perkin Elmer. All the labware was scrupulously cleaned and labeled to ensure that no contamination took place. All glassware was acid washed and rinsed in distilled water before use.
The AA manual specifies the following parameters for Mn:

- Wavelength: 279.8 A

- Slit height: 0.2 nm

- Flame: Acetylene-air

- Modifier: 0.2 % Calcium chloride in 1 % Hydrochloric acid

- Linear range: 2 - 20 parts per million (ppm)

A set of solutions was necessary for adjusting and calibrating the AA unit. The standards were made by diluting stock manganese solutions made especially for AA work. The stock

solutions come in a matrix (the matrix is the concentration of companion ions and acids resulting from dissolving the elemental salts used to manufacture the standard). The stock solutions were purchased from Fisher Scientific.

## a. Sample Preparation

The samples were digested in a beaker with 5ml concentrated nitric acid. The digested samples were diluted to a concentration within the linear absorbance range of the for the element. Dilution was accomplished by adding a modifier solution as indicated by the Zeeman 5000 manual. The diluted sample was transferred to a Nalgene bottle and held for analysis. At the same time a blank solution (without any sample in it) was also prepared. The blank is used as a reference to zero the machine before calibrating.

The AA machine was calibrated to show concentration. Each piece of the sample is prepared for analysis in a calculated volume. The obtained Mn concentration was plotted against position in the solid.

## 4. Results

A number of experimental runs were completed. Many of the ampoules cracked during the compacting of the material. Also the first set of samples, that were solidified showed gaps and bubbles. The samples from completed experiments were analysed and the obtained concentration was plot against distance. The results are shown in the figures (2.13-2.15). A polynomial of degree four was used to fit the data. The concentration profiles are similar to that predicted by theory. The data is being standardized. The standardized concentration profiles will be compared to theoretical concentration profiles. Preliminary comparisons show that a Soret coefficient of $5 \times 10^{-8}$ cm$^2$/s/°C and a diffusion coefficient of $1 \times 10^{-5}$ cm$^2$/s gives a concentration profile like that obtained by experiment.

The experimental concentration profiles are not constant in the middle of the furnace as predicted by theory. This could be because the theoretical model used a constant temperature gradient, but the actual concentration gradient of the furnace is not constant. The difference in the concentration profile obtained by experiment and that obtained by theoretical calculation may be attributed to a number of reasons:

- The initial concentration may not be uniform.

- There might be a loss of material during the preparation of the sample.

- Small convection cells might alter the concentration during the experiment.

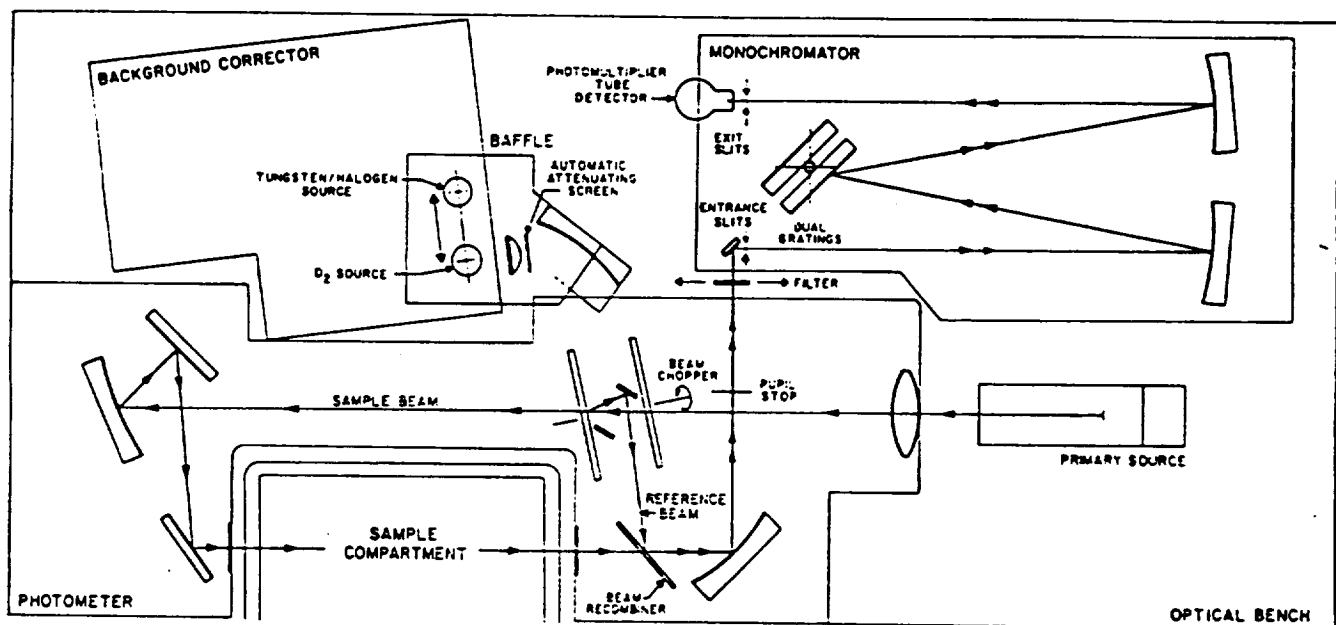- Gravity effects cannot be neglected.

Figure 2.12: A schematic of the optical system of the Perkin-Elmer model 5000 atomic absorption spectrophotometer.
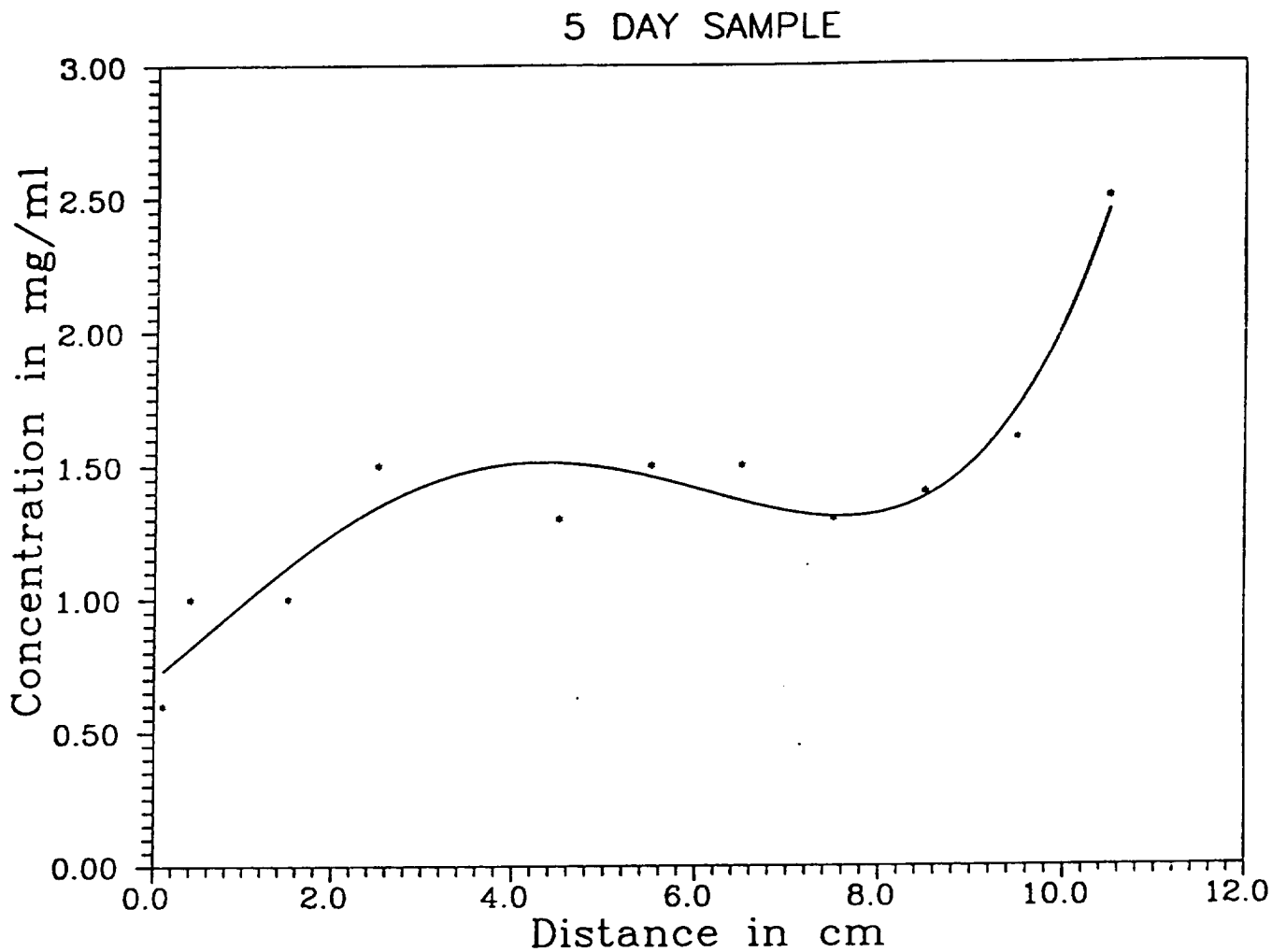
**Figure 2.13:** Concentration gradient of Mn along the length of the sample (the far end is the hot end).
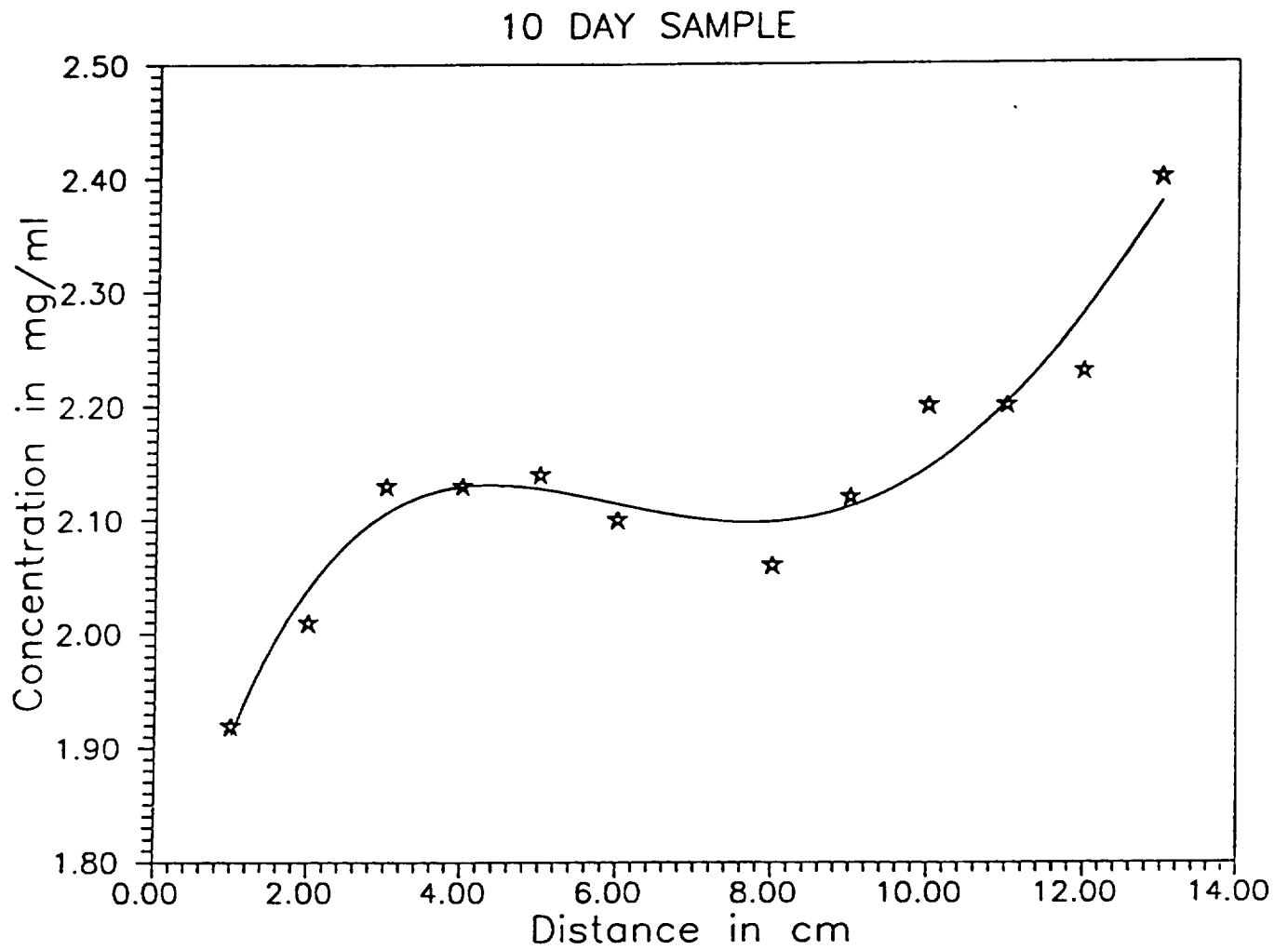
## 10 DAY SAMPLE



Figure 2.14: Concentration gradient of Mn along the length of the sample (the far end is the hot end).
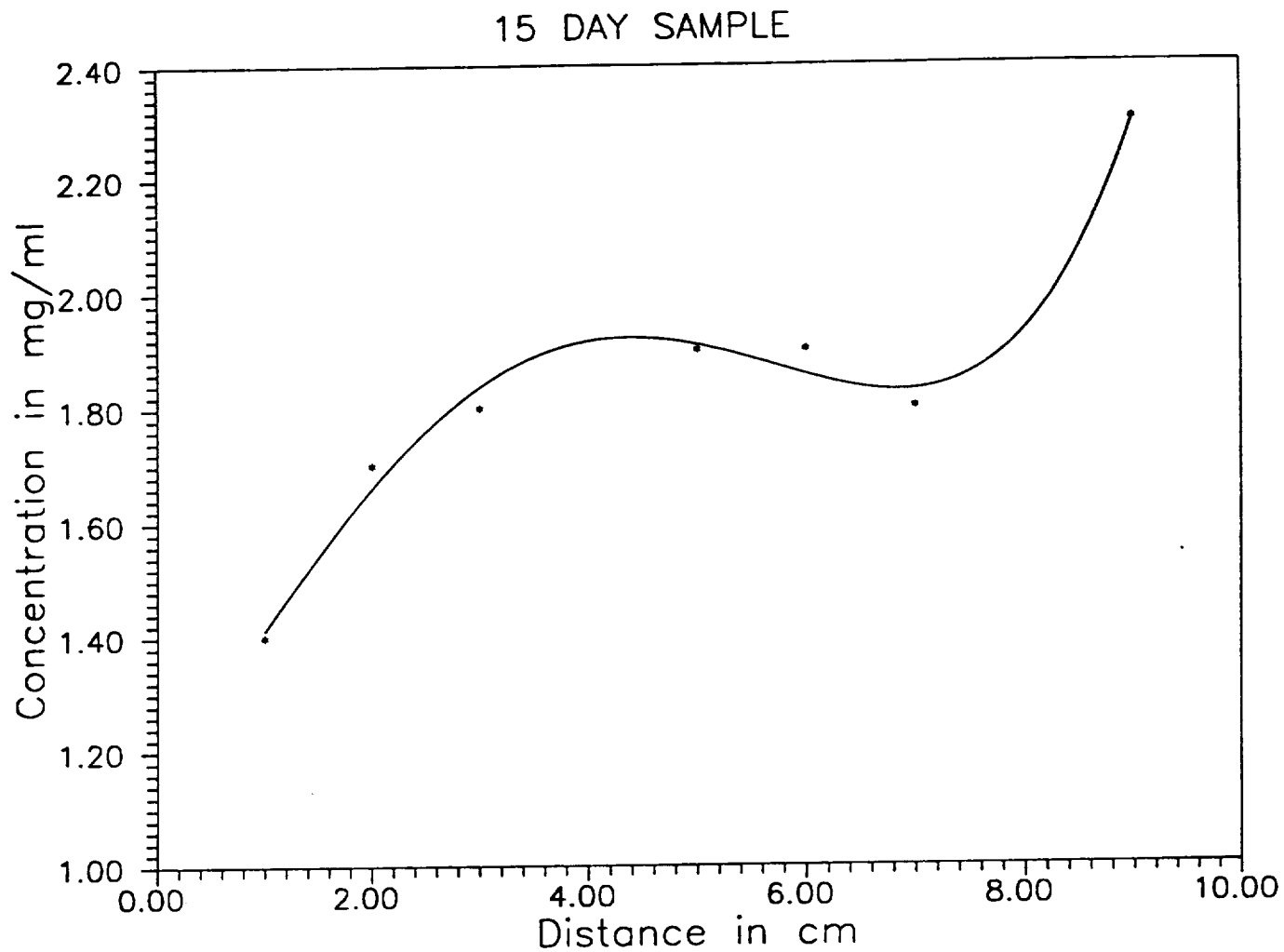
**Figure 2.15:** Concentration gradient of Mn along the length of the sample (the far end is the hot end).

## C. Plans

1. Some more experiments will be conducted for the shorter time periods.

2. The thermal modeling of the diffusion furnace will be completed so as to determine the theoretical temperature profile of the furnace.

3. The actual temperature profile of the furnace will be used in the theoretical modeling of the problem.

4. The data obtained from experiments will be compared to the theoretical data.

5. An estimate of the Soret coefficient will be obtained.

# References

1. R. Elliot, Eutectic Solidification Processing, Butterworth, London (1983).

2. C. A. Adams, Science and Technology of Undercooled Melt, P. R. Sahm, H. Jones and C. M. Adams, eds., Martinus Nijhoff, Dedrecht (1986).

3. W. H. Brandt, J. Appl. Phys. 16 (1945) 139.

4. C. Zener, Trans. AIME 167 (1946) 550.

5. M. Hillert, Jernkontorets Ann. 144 (1960) 520.

6. W. A. Tiller, Liquid metals and Solidification, ASM, Metals Park, OH (1958) 276.

7. K. A. Jackson and J. D. Hunt, Trans. AIME 236 (1966) 1129.

8. V. Baskaran and W. R. Wilcox, J. Crystal Growth 67 (1984) 343.

9. W. R. Wilcox, K. R. Doddi, M. Nair and D. J. Larson, Adv. Space Res. (1983), 79.

10. P. S. Ravishankar, W. R. Wilcox and D. J. Larson, Acta Met. 28 (1980) 1583.

11. M. Nair, T. W. Fu, W. R. Wilcox, K. R. Doddi and P. S. Ravishankar, Materials Processing in Reduced Gravity Environment of space, Proceedings of the Mat. Res. Soc. Annual Meeting, Editor Guy E. Rindone, Pergamon, NY (1982) 533-541.

12. S. Chandrasekhar, G. F. Eisa, and W. R. Wilcox, J. Crystal Growth 76 (1986) 485-488.

13. G. F. Eisa, W. R. Wilcox and G. Busch, J. Crystal Growth 78, 156-174.

14. W. Slavin, Atomic Absorption Spectroscopy, Wiley and sons (1968).

15. B. Welz, Atomic Absorption Spectroscopy, Verlag Chemie, (1976).

# III. EFFECT OF CONVECTION ON THE MICROSTUCTURE OF MnBi/Bi EUTECTIC

JAYSHREE SETH

## SUMMARY

The objective of this project is to develop a numerical model to study the influence of convective flow on the microstructure of MnBi/Bi lamellar eutectic when the MnBi phase projects out into the melt.

The model will utilize a central finite difference approach. A steady well developed laminar flow parallel to the solidification interface and perpendicular to the lamellae will be considered. The determination of the velocity profile as the melt moves over the lamellae requires the solving of the Navier-Stokes equation. Once the velocity profile has been calculated, the governing mass transfer equation, including the effect of convective flow, will be numerically solved to yield the solute concentration in the diffusion field in front of the growing interface. From this we will calculate the influence of convection on lamellar spacing using the minimum supercooling criterion of Hunt and Jackson [1].

## A. INTRODUCTION

The primary motivation for this work arises from experiments on solidification in the reduced gravity environment of space. These showed marked structural difference from identically processed earth-grown samples. The difference has been attributed to the absence of convective currents at low g as compared to conditions on earth.

Baskaran [2] developed a two dimensional numerical model to study the effect of convection on the lamellar spacing of MnBi/Bi eutectic. Eisa [3] performed theoretical work using the numerical results for the convection field with more intense convection and developed a correlation for the effect of convection on the interfacial undercooling. Chandrasekhar [4] performed numerical analysis to study the effect of convection on the rod spacing. Caram [5] developed a three dimensional numerical model for the influence of convection on the eutectic microstructure. He approximated each rod's cross section by a circle as done by Jackson and Hunt [1]. Chandrasekhar [4] performed decantation experiments wherein the remaining melt was poured off during the slidification of the MnBi/Bi eutectic. He found that the MnBi fibers were projecting ahead of the Bi matrix. In the present work a lamellar structure is being studied rather than a rod structure for computational ease; the diffusional domain of a lamellar eutectic is two dimensional rather than three dimensional as is the case of a rod eutectic. The resulting observations are expected to hold for a rod structure in a semi-quantative sense.

## B. PROGRESS

Some of the relevant literature was reviewed [1,2,3,4,5]. During an eutectic solidification as the solid phases grow they reject atoms to the melt and as a result there is a variation of liquid composition along the interface. Mass transfer in the absence of any convective flow is governed by the following differential equation

$$\nabla^2 C + (V/D)\,(\partial C/\partial Z) = 0$$

where C is the composition of the melt, V the rate of displacement of the solid-liquid interface and D is the diffusion coefficient of the solute. Jackson and Hunt [1] obtained an analytical solution for the concentration field. They used it to calculate the average undercooling at the interface and the rod spacing.

To calculate the velocity profile when the melt creeps over the projecting phase, the Navier-Stokes equation has to be solved. A transverse flow is assumed across the interface to simulate convection. The boundary conditions imposed on the velocity field are shown in Fig. 2. The problem domain is chosen such that it represents the smallest region which will satisfy the periodicity condition. The various boundary conditions applicable while solving for the diffusion field are shown in Fig. 3. The average concentration of the interfacial liquid over each solid phase, under the influence of convection can thus be calculated using the mass balance equation,

$$D\nabla^2 C - \upsilon \cdot \nabla C = 0$$

D is the diffusion coefficient of the solute. $\upsilon$ is the velocity profile obtained from solving the Navier Stokes equation.

## C. PLANS

1) Propose and justify simplifying assumptions in order to reduce computational difficulties.
2) Understand the working of the software 'FLUENT' and develop ways of incorporating it for the given problem.
3) Write code for solving the mass transfer equation

## REFERENCES

1. Jackson, K.A., and Hunt, J.D., Trans, AIME 2368 (1966) 1129.

2. Baskaran, V., and Wilcox, W.R., J. Crystal Growth, 67(1984)343.

3. Eisa, G. F., "Effect of convection on the microstructure of MnBi-Bi eutectic solidified from melt," Ph.D thesis, Clarkson University, Potsdam, NY(1985).

4. Chandrasekhar, S., "Effect of convection on the microstructure of MnBi-Bi eutectic," Ph.D thesis, Clarkson University, Potsdam, NY(August 1987).

5. Caram, R., Chandrasekhar, S., and Wilcox, W.R., "Influence of convection on rod spacing of eutectics" submitted for publication (J. Crystal Growth)

β-phase

α-phase

α
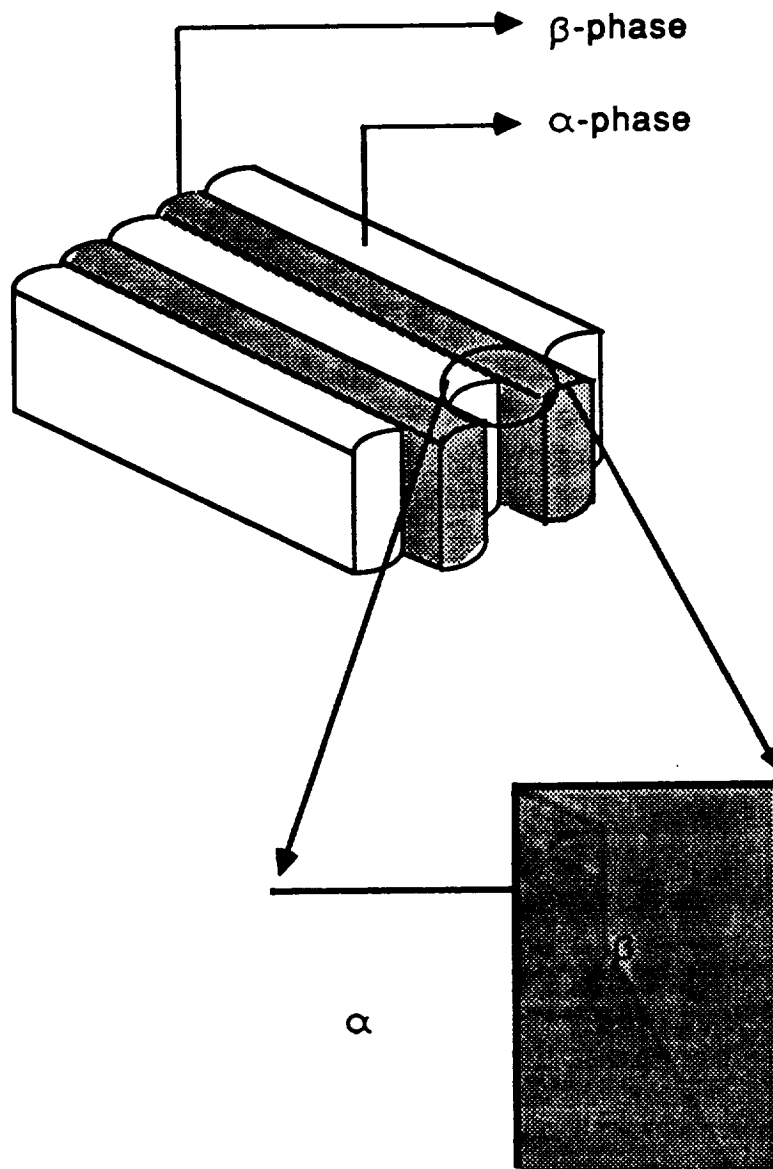
One phase projecting into the melt. (Lamellar eutectic)
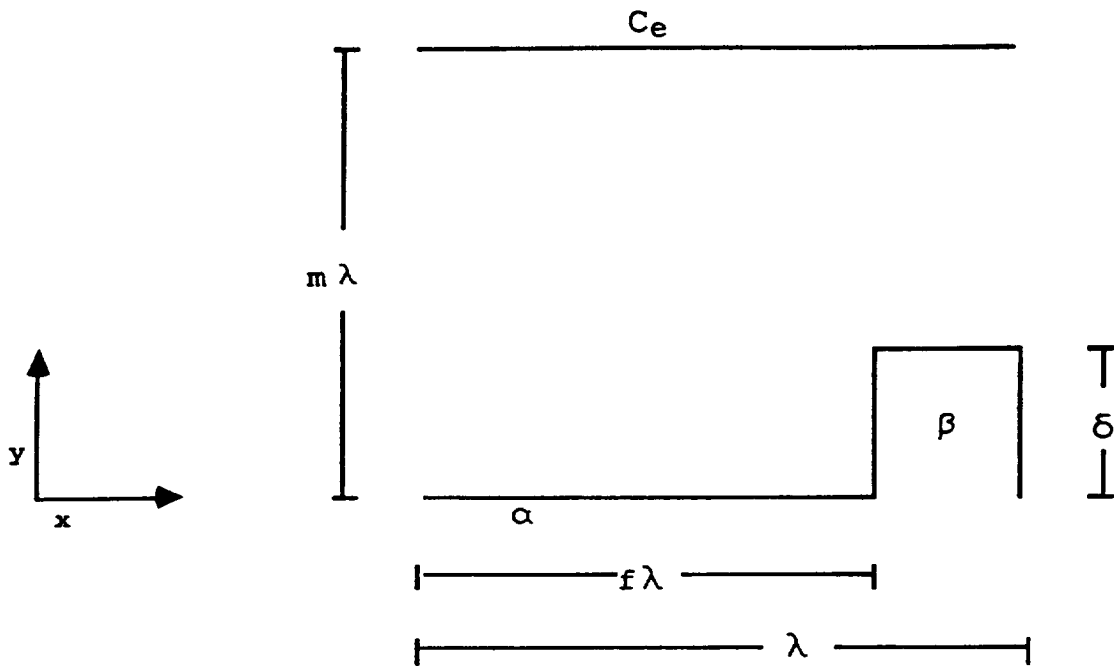
Fig. 1
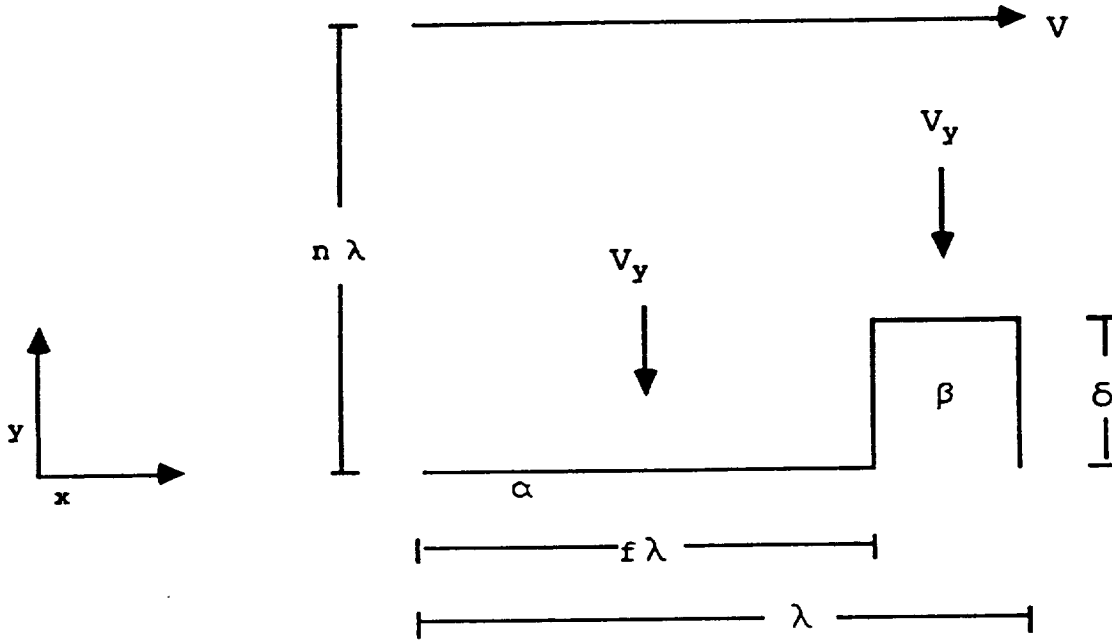
NAVIER STOKES EQUATION (x component)

$$V_x\left(\frac{\partial V_x}{\partial x}\right) + V_y\left(\frac{\partial V_x}{\partial y}\right) = \mu\left(\frac{\partial^2 V_x}{\partial x^2} + \frac{\partial^2 V_x}{\partial y^2}\right)$$

Boundary conditions

| All x | $y = n\delta$ | $V_x = V_\infty$, $V_y = -V$ | (Far field condition) |
| $0 \le x \le f\lambda$ | $y = 0$ | $V_x = 0$, $V_y = -V$ | (no slip condition) |
| $f\lambda \le x \le \lambda$ | $y = \delta$ | $V_x = 0$, $V_y = -V$ | (no slip condition) |
| $x = f\lambda$ | $0 \le y \le \delta$ | $V_x = 0$, $V_y = -V$ | (no side growth) |

$$V_{x=0} = V_{x=\lambda} \qquad \text{all y} \qquad \text{(periodicity condition)}$$

Fig 2. Problem domain for velocity profile.

## MASS TRANSFER EQUATION

$$D\nabla^2 C - \vec{v} \cdot \nabla C = 0$$

### Boundary conditions

| | | | |
|---|---|---|---|
| All x | $y = m\lambda$ | $C = C_e$ | (infinity condition) |
| $0 \leq x \leq f\lambda$ | $y = 0$ | $D(\frac{\partial C}{\partial y}) = V(C_i\text{-}C_\alpha)$ | (over $\alpha$ phase) |
| $f\lambda \leq x \leq \lambda$ | $y = \delta$ | $D(\frac{\partial C}{\partial y}) = V(C_i\text{-}C_\beta)$ | (over $\beta$ phase) |
| $x = f\lambda$ | $0 \leq y \leq \delta$ | $(\frac{\partial C}{\partial x}) = 0$ | (no side growth) |

$$C_{x=0} = C_{x=\lambda} \qquad \text{all y} \qquad \text{(periodicity condition)}$$

Fig 3. Problem domain for concentration profile.